

## RESEARCH ARTICLE

# Vimentin intermediate filaments control actin stress fiber assembly through GEF-H1 and RhoA

Yaming Jiu<sup>1,\*</sup>, Johan Peränen<sup>2</sup>, Niccole Schaible<sup>3</sup>, Fang Cheng<sup>4,5</sup>, John E. Eriksson<sup>4,5</sup>, Ramaswamy Krishnan<sup>3</sup> and Pekka Lappalainen<sup>1,\*</sup>

## ABSTRACT

The actin and intermediate filament cytoskeletons contribute to numerous cellular processes, including morphogenesis, cytokinesis and migration. These two cytoskeletal systems associate with each other, but the underlying mechanisms of this interaction are incompletely understood. Here, we show that inactivation of vimentin leads to increased actin stress fiber assembly and contractility, and consequent elevation of myosin light chain phosphorylation and stabilization of tropomyosin-4.2 (see Geeves et al., 2015). The vimentin-knockout phenotypes can be rescued by re-expression of wild-type vimentin, but not by the non-filamentous 'unit length form' vimentin, demonstrating that intact vimentin intermediate filaments are required to facilitate the effects on the actin cytoskeleton. Finally, we provide evidence that the effects of vimentin on stress fibers are mediated by activation of RhoA through its guanine nucleotide exchange factor GEF-H1 (also known as ARHGEF2). Vimentin depletion induces phosphorylation of the microtubule-associated GEF-H1 on Ser886, and thereby promotes RhoA activity and actin stress fiber assembly. Taken together, these data reveal a new mechanism by which intermediate filaments regulate contractile actomyosin bundles, and may explain why elevated vimentin expression levels correlate with increased migration and invasion of cancer cells.

**KEY WORDS:** Vimentin, Intermediate filament, Actin, Stress fiber, RhoA, GEF-H1

## INTRODUCTION

The actin cytoskeleton contributes to diverse cell biological, developmental, physiological and pathological processes in multicellular animals. Precisely regulated polymerization of actin filaments provides a force for generating membrane protrusions and invaginations during cell morphogenesis, migration and endocytosis. Actin and myosin II filaments also form contractile structures, where the force is generated by movement of myosin


motor domains along actin filaments. The most prominent contractile actomyosin structures in non-muscle cells are stress fibers. Beyond cell migration and morphogenesis, stress fibers contribute to adhesion, mechanotransduction, endothelial barrier integrity and myofibril assembly (Burridge and Wittchen, 2013; Sanger et al., 2005; Tojkander et al., 2015; Wong et al., 1983; Yi et al., 2012). Stress fibers can be classified into three categories, which differ in their protein compositions and assembly mechanisms. Dorsal stress fibers are non-contractile actin bundles that are assembled through VASP- and formin-catalyzed actin filament polymerization at focal adhesions. Transverse arcs are contractile actomyosin bundles that are generated from the Arp2/3- and formin-nucleated lamellipodial actin filament network. These two stress fiber types serve as precursors for ventral stress fibers, which are mechanosensitive actomyosin bundles that are linked to focal adhesions at their both ends (Hotulainen and Lappalainen, 2006; Tojkander et al., 2011, 2015; Burnette et al., 2011; Skau et al., 2015; Tee et al., 2015). In addition to actin and myosin II, stress fibers are composed of a large array of actin-regulating and signaling proteins, including the actin filament cross-linking protein  $\alpha$ -actinin and the actin filament-decorating tropomyosin proteins (Tojkander et al., 2012).

The Rho family small GTPases are central regulators of actin dynamics and organization in eukaryotic cells. Amongst these, RhoA in particular has been linked to generation of contractile actomyosin stress fibers. RhoA drives the assembly of focal adhesion-bound actomyosin bundles by inhibiting proteins that promote actin filament disassembly, by activating proteins that catalyze actin filament assembly at focal adhesions and by stimulating myosin II contractility through activation of ROCK kinases that catalyze myosin light chain phosphorylation (Heasman and Ridley, 2008). RhoA can be activated by Rho-guanine nucleotide exchange factors (Rho-GEFs), including Ect2, GEF-H1 (also known as ARHGEF2), MyoGEF (also known as PLEKHG6) and LARG (also known as ARHGEF12), which stimulate the GDP-to-GTP exchange in the nucleotide-binding pocket of RhoA. From these, Ect2 has a well-established role in the formation of contractile actomyosin structures at mitotic exit (Matthews et al., 2012), whereas the microtubule-associated GEF-H1 contributes to cell migration, cytokinesis and vesicular traffic (Ren et al., 1998; Nalbant et al., 2009; Birkenfeld et al., 2007; Pathak et al., 2012).

In addition to mechanosensitive interplay with focal adhesions and the plasma membrane, stress fibers interact with other cytoskeletal elements; microtubules and intermediate filament (IFs) (Huber et al., 2015; Jiu et al., 2015). IFs are stable but resilient cytoskeletal structures that provide structural support for cells and serve as signaling platforms. Vimentin and keratins are the major IF proteins in mesenchymal and epithelial cells, respectively (Eriksson et al., 2009; Snider and Omary, 2014; Loschke et al.,

<sup>1</sup>Institute of Biotechnology, P.O. Box 56, University of Helsinki, Helsinki 00014, Finland. <sup>2</sup>Faculty of Medicine, P.O. Box 63, University of Helsinki, Helsinki 00014, Finland. <sup>3</sup>Department of Emergency Medicine, Beth Israel Deaconess Medical Center, Harvard Medical School, Boston, MA 02215, USA. <sup>4</sup>Cell Biology, Biosciences, Faculty of Science and Engineering, Åbo Akademi University, FI-20520 Turku, Finland. <sup>5</sup>Turku Centre for Biotechnology, University of Turku and Åbo Akademi University, POB 123, FI-20521 Turku, Finland.

\*Authors for correspondence (yaming.jiu@helsinki.fi; pekka.lappalainen@helsinki.fi)

 Y.J., 0000-0002-8601-8820; P.L., 0000-0001-6227-0354

This is an Open Access article distributed under the terms of the Creative Commons Attribution License (<http://creativecommons.org/licenses/by/3.0>), which permits unrestricted use, distribution and reproduction in any medium provided that the original work is properly attributed.

2015). Vimentin can interact with actin filaments both directly through its C-terminal tail and indirectly through the plectin cytoskeletal cross-linking protein (Esue et al., 2006; Svitkina et al., 1996). Furthermore, IFs display robust interactions with microtubules in cells (Huber et al., 2015). Importantly, several studies demonstrated that disruption of the actin cytoskeleton affects subcellular localization of the IF network in cells (Hollenbeck et al., 1989; Dupin et al., 2011; Jiu et al., 2015). More precisely, transverse arcs and ventral stress fibers interact with vimentin IFs through plectin, and retrograde flow of these contractile actomyosin bundles transports vimentin filaments from the leading edge towards the perinuclear region of the cell (Jiu et al., 2015). IFs can reciprocally affect actin-dependent processes such as cell adhesion and migration, because vimentin depletion results in impaired cell migration and pronounced stress fiber-attached focal adhesions (Bhattacharya et al., 2009; Eckes et al., 1998, 2000; Mendez et al., 2010). Moreover, keratin-8–keratin-18 displays interplay with Solo (also known as ARHGEF40), a RhoA-GEF, to control force-induced RhoA activation and consequent stress fiber assembly (Fujiwara et al., 2016). Finally, depletion of the cytoskeletal cross-linker, plectin, leads to similar abnormalities in focal adhesions and actin-dependent processes compared to vimentin depletion (Abrahamsberg et al., 2005; Andra et al., 1998). The effects of IFs and plectin on focal adhesions and the actin cytoskeleton have been so far linked to integrin-driven activation of focal adhesion kinase (FAK, also known as PTK2) and its downstream signaling cascade (Gregor et al., 2014). However, the effects of IFs on the stress fiber network and the underlying mechanisms have remained obscure. In addition, the principles by which vimentin controls cell adhesion, migration and invasion are incompletely understood.

Here, we report a vimentin-dependent downregulation of the stress fiber network in osteosarcoma cells and in fibroblasts. We show that depletion of vimentin results in an increased activation and phosphorylation of GEF-H1. This leads to an increase in the levels of active RhoA and consequent stress fiber assembly. Thus, our work proposes a novel pathway by which vimentin IFs regulate actin dynamics in cells.

## RESULTS

### Vimentin filaments inhibit the assembly of contractile stress fibers

It is now well established that vimentin expression correlates with increased cell motility and invasiveness, which in turn are associated with actin dynamics. To this end, our recent work on U2OS cells revealed that actin transverse arcs transport vimentin filaments towards the cell center, whereas the vimentin IFs resist the retrograde movements of these contractile actomyosin bundles (Jiu et al., 2015). Interestingly, the vimentin-knockout U2OS cells also display thicker stress fibers as detected by phalloidin staining, and more intense tropomyosin 4.2 (for an explanation of tropomyosin nomenclature, see Geeves et al., 2015) staining compared to control cells (Fig. 1A). Tpm4.2 is a central stress fiber component that is involved in myosin II recruitment to stress fibers (Tojkander et al., 2011). To validate these findings, we performed western blot analysis on vimentin-knockout and control cells. Consistent with the immunofluorescence data, vimentin depletion resulted in a significant increase in Tpm4.2 protein levels, while the actin levels were only mildly increased upon vimentin depletion (Fig. 1C,D). The interplay between vimentin and Tpm4.2 is not restricted to U2OS cells, because immunofluorescence microscopy and western blot experiments also demonstrated increased Tpm4.2 levels in

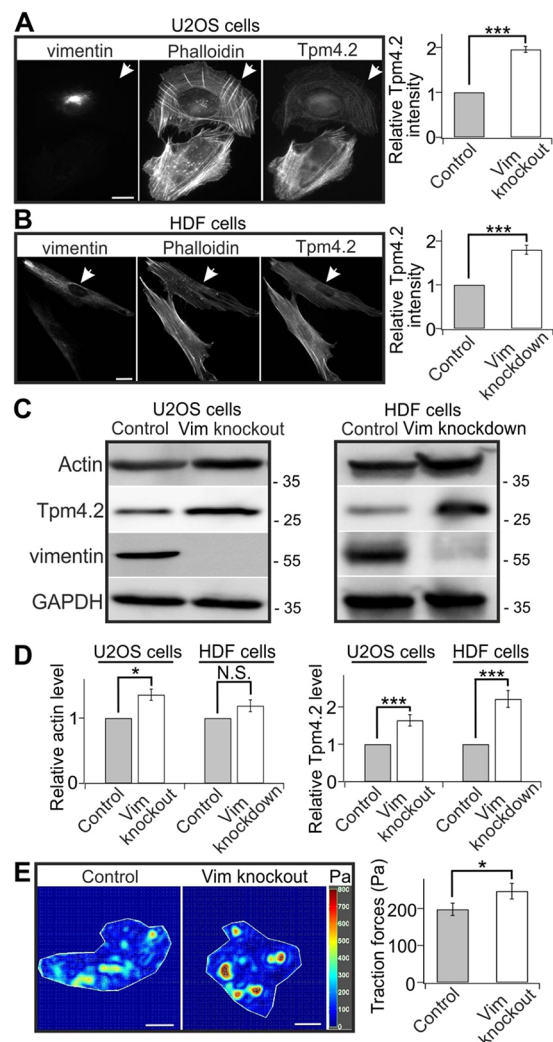


**Fig. 1. Vimentin depletion induces stress fiber assembly.** (A,B) The intensities of Tpm4.2 and F-actin (as detected by fluorescent phalloidin) are increased in vimentin-knockout U2OS cells (A) and knockdown HDF cells generated using a vimentin siRNA pool (B). Panels on the left show representative images of control (arrowheads) and vimentin-depleted cells that were co-cultured on same plates. Panels on the right show the quantifications of normalized relative Tpm4.2 fluorescent intensities in control (A, 32 cells from nine images; B, 32 cells from nine images) and vimentin-knockout or knockdown cells (A, 38 cells from nine images; B, 33 cells from nine images). Mean intensity values of control and knockout or knockdown cells from each image were used for statistical analysis. \*\*\* $P < 0.001$  (paired  $t$ -test). (C) Western blot analysis of actin and Tpm4.2 protein levels in control and vimentin-depleted U2OS (left panel) and HDF (right panel) cells. The blots were also probed with vimentin antibody to confirm that the vimentin-knockout U2OS cell culture is not contaminated by wild-type U2OS cells and to verify efficiency of vimentin depletion in siRNA-treated HDF cells, and with GAPDH antibody to control equal sample loading. Molecular masses in kilodaltons (kDa) are indicated in the blots. (D) Quantification of the relative levels of actin (left panel) and Tpm4.2 (right panel) normalized to internal control GAPDH from five western blots. \* $P < 0.05$ , \*\*\* $P < 0.001$ ; N.S., not significant (paired  $t$ -test). (E) Vimentin-knockout results in increased cell contractility detected by traction force microscopy. Panels on the left show representative force maps of control and vimentin-knockout cells grown on 25 kPa polyacrylamide dishes with fluorescent nanobeads. The panel on the right shows the quantification of traction forces (root mean square traction) in control cells ( $n=47$ ) and vimentin-knockout cells ( $n=47$ ) from three independent experiments. \* $P < 0.05$  (Mann–Whitney–Wilcoxon rank-sum test). The data are presented as mean  $\pm$  s.e.m. Scale bars: 10  $\mu$ m.

RNA interference (RNAi)-induced vimentin-knockdown human dermal fibroblasts (HDFs) (Fig. 1A–D).

Quantitative real-time RT-PCR (qRT-PCR) revealed no significant differences in Tpm4.2 mRNA levels between control and vimentin-knockout cells (Fig. S1A), indicating that vimentin does not regulate Tpm4.2 at the transcriptional level. We thus examined possible effects of vimentin on the stability of Tpm4.2 protein by treating U2OS cells with cycloheximide (CHX) to inhibit protein translation. This experiment showed that Tpm4.2 was very stable in CHX-treated vimentin-knockout cells during the 24 h experimental period, whereas in control cells Tpm4.2 protein levels were drastically diminished after a 6 h CHX-treatment (Fig. S1B). Moreover, global disruption of actin stress fiber network upon treatment with the myosin II inhibitor, blebbistatin, resulted in a significant decrease in the Tpm4.2 protein levels (Fig. S1C), indicating that Tpm4.2 protein is unstable and becomes degraded in the absence of stress fibers. Thus, lack of vimentin leads to an increased assembly and stability of stress fibers, and this consequently results in a diminished turnover of the Tpm4.2 protein.

Because Tpm4.2 localizes specifically to myosin II-containing transverse arcs and ventral stress fibers (Tojkander et al., 2011), we hypothesized that loss of vimentin may also affect contractility of stress fibers. Contractile force measurements performed using traction force microscopy revealed that vimentin-knockout cells exert ~25% greater traction forces compared to control cells (Fig. 1E). To examine the activity of myosin II, control and vimentin-knockout cells were stained with an antibody detecting phosphorylated (Thr18/Ser19) myosin light chain (P-MLC; recognizing phosphorylated myosin light chain 2). Lack of vimentin resulted in ~2-fold increases in P-MLC intensity and total P-MLC levels when cells were grown on glass, or on a softer 33 kPa polyacrylamide substrates (Fig. 2A,B). Conversely, overexpression of vimentin reduced the intensities of Tpm4.2 and P-MLC (Fig. S2C,D).

To examine whether the filamentous form of vimentin is necessary for its effects on stress fibers, we performed knockout-rescue experiments with wild-type vimentin and with the ‘unit length filament’ (ULF) vimentin mutant Y117L, which preserves vimentin interaction with other components of the cytoskeleton, but cannot assemble into filaments (Meier et al., 2009). These experiments revealed that whereas full-length GFP–vimentin can rescue the stress fiber phenotype, the knockout cells expressing ‘non-polymerizable’ ULF–GFP displayed similar intensities of Tpm4.2 and P-MLC compared to non-transfected vimentin-knockout cells (Fig. 2C–F). Taken together, these data show that intact vimentin IFs diminish stress fiber assembly, contractility, myosin light chain phosphorylation and Tpm4.2 stability.

### Vimentin depletion results in increased levels of active RhoA

RhoA regulates myosin light chain phosphorylation and activities of several actin-binding proteins to promote stress fiber contractility and assembly (Guilluy et al., 2011a,b; Lessey et al., 2012). We thus hypothesized that levels of active RhoA may be regulated by vimentin. By using G-LISA, a small GTPase activation assay, we discovered that absence of vimentin significantly increased the level of active GTP-bound, RhoA in U2OS cells (Fig. 3A). This effect could be rescued by expression of full-length vimentin, but not by the non-polymerizable ULF fragment, demonstrating that the presence of filamentous vimentin is required for suppression of RhoA activity (Fig. 3A). Based on immunostainings, western blot analysis and qRT-PCR, we observed that neither the subcellular

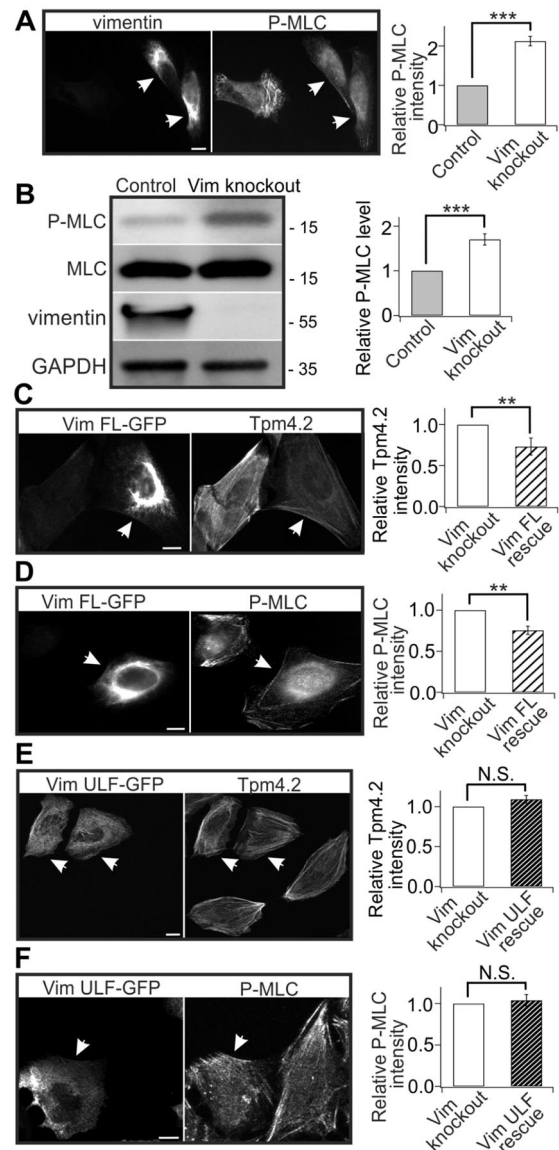


Fig. 2. See next page for legend.

localization nor the total protein levels and mRNA levels of RhoA were affected by vimentin depletion (Fig. 3B,C; Fig. S3D). This suggests that vimentin specifically controls the ratio of GTP- versus GDP-loaded RhoA. Vimentin also exerted its effects on stress fibers through RhoA activity; expression of dominant negative (DN)-RhoA blocked the augmentation of Tpm4.2 and P-MLC levels in both vimentin-knockout cells (Fig. 3D,E) and control U2OS cells (Fig. S3A–C). It is, however, important to note that DN-RhoA can compete for binding to Rho GDP dissociation inhibitors (GDIs) and may thus have different effects in cells compared to RhoA depletion. Taken together, these data demonstrate that vimentin filaments inhibit stress fiber assembly by downregulating RhoA.

### Vimentin regulates RhoA through GEF-H1

Because IFs associate with microtubules (Leduc and Etienne-Manneville, 2015), we investigated by RNAi whether the microtubule-associated RhoA exchange factor GEF-H1 (Ren et al., 1998; Krendel et al., 2002) could mediate the cross-talk between vimentin and RhoA signaling during stress fiber formation and contractility. With appropriate siRNA oligonucleotide, we

**Fig. 2. The filamentous form of vimentin is necessary for its effects on stress fiber assembly.** (A) The intensity of P-MLC is increased in vimentin-knockout U2OS cells. The panel on the left shows representative images of control (arrowheads) and vimentin-knockout cells that were co-cultured on same plates. The panel on the right shows the quantification of normalized relative P-MLC fluorescent intensities in control (35 cells from nine images) and vimentin-knockout cells (37 cells from nine images). Mean intensity values of control and knockout cells from each image were used for statistical analysis.  $***P < 0.001$  (paired *t*-test). (B) Western blot analysis of P-MLC levels in control and vimentin-knockout U2OS cells (left panel). The blots were also probed with vimentin antibody to confirm that the vimentin-knockout cell culture is not contaminated by wild-type cells, and with GAPDH antibody to verify equal sample loading. Molecular masses in kilodaltons (kDa) are indicated in the blots. The panel on the right shows the normalized relative levels of P-MLC compared to the total MLC protein levels from three western blots.  $***P < 0.001$  (paired *t*-test). (C,D) Full-length (FL) vimentin rescued the increase of Tpm4.2 (C) and P-MLC (D) levels induced by vimentin depletion. Panels on the left show representative images of vimentin-knockout cells expressing FL-vimentin–GFP (arrowheads) and non-transfected vimentin-knockout cells. Panels on the right show the quantifications of normalized relative Tpm4.2 (C, 33 control cells from eight images; 35 vimentin-knockout cells from eight images) and P-MLC (D, 26 control cells from eight images; 28 vimentin-knockout cells from eight images) fluorescence intensities. Mean intensity values of control and vimentin overexpression cells from each image were used for statistical analysis.  $**P < 0.01$  (paired *t*-test). (E,F) ‘Unit length form’ vimentin is not able to rescue the increase of Tpm4.2 (E) and P-MLC (F) levels induced by vimentin depletion. Panels on the left show representative images of vimentin-knockout cells expressing ULF-vimentin–GFP (arrowheads) and non-transfected vimentin-knockout cells. Panels on the right show the quantifications of normalized relative Tpm4.2 (E, 27 control cells from eight images; 32 knockout cells from eight images) and P-MLC (F, 29 control cells from eight images; 28 knockout cells from eight images) fluorescence intensities. Mean intensity values of control and ULF vimentin overexpression cells from each image were used for statistical analysis. The data are presented as mean  $\pm$  s.e.m. N.S., not significant. Scale bars: 10  $\mu$ m.

succeeded in efficiently depleting GEF-H1 from U2OS cells (Fig. 4A). Incubation of cells for 3 days with siRNAs against GEF-H1 led to changes in cell morphology and to a dramatic decrease in the number of stress fibers (data not shown), supporting the known role of GEF-H1 in stress fiber assembly. Strikingly, by using the G-LISA method, we found that silencing of GEF-H1 significantly diminished levels of active RhoA in both control and vimentin-knockout cells (Fig. 4B). This result was further confirmed with a different siRNA oligonucleotide against GEF-H1 (Fig. S3F,G). Thus, GEF-H1 appears to be the predominant GEF that activates RhoA in U2OS cells.

To elucidate the mechanism by which GEF-H1 is involved in vimentin-mediated suppression of RhoA, we assessed the interaction of endogenous vimentin and GEF-H1 by a co-immunoprecipitation assay. This experiment provided evidence that GEF-H1 either directly or indirectly interacts with vimentin (Fig. 4C). Furthermore, in cells transfected with vimentin–mCherry, and stained with anti-GEF-H1 and tubulin antibodies, vimentin filaments often aligned with GEF-H1-containing microtubules (Fig. 4D). We next examined whether vimentin regulates the localization or dynamics of GEF-H1 in cells. Immunofluorescence microscopy experiments demonstrated that GEF-H1 colocalized similarly with microtubules in both control and vimentin-knockout cells (Fig. 4E), whereas the dynamics of GEF-H1 were moderately increased in vimentin-knockout cells compared to control cells. Fluorescence recovery after photobleaching (FRAP) experiments on cells expressing GFP–GEF-H1 revealed a highly dynamic association of GEF-H1 with filamentous structures that are likely to represent microtubules. However, the recoveries of both the predominant dynamic population (half-time 1) and the smaller slow

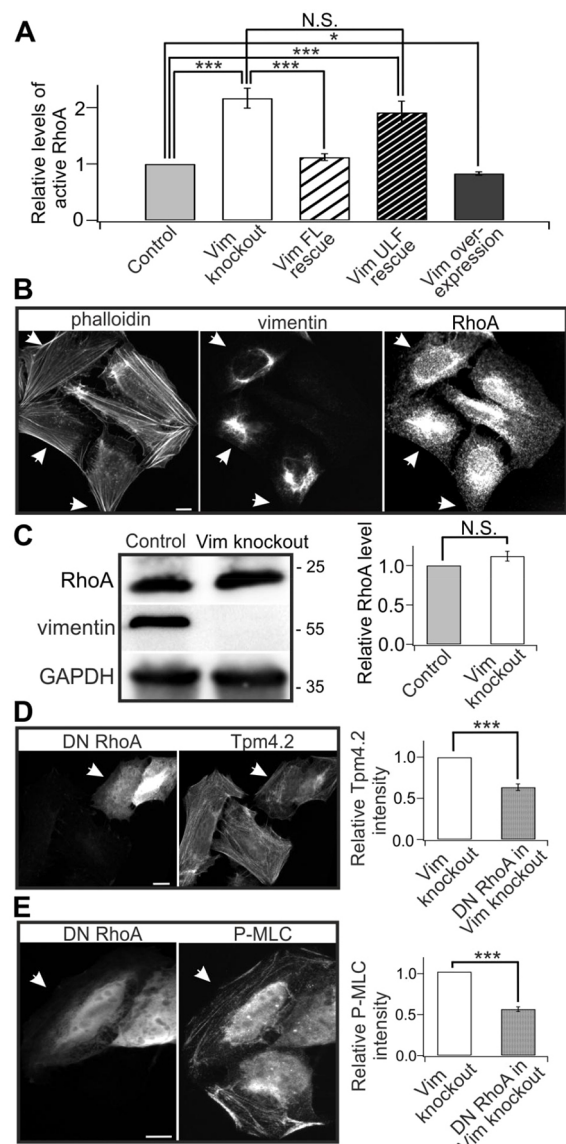
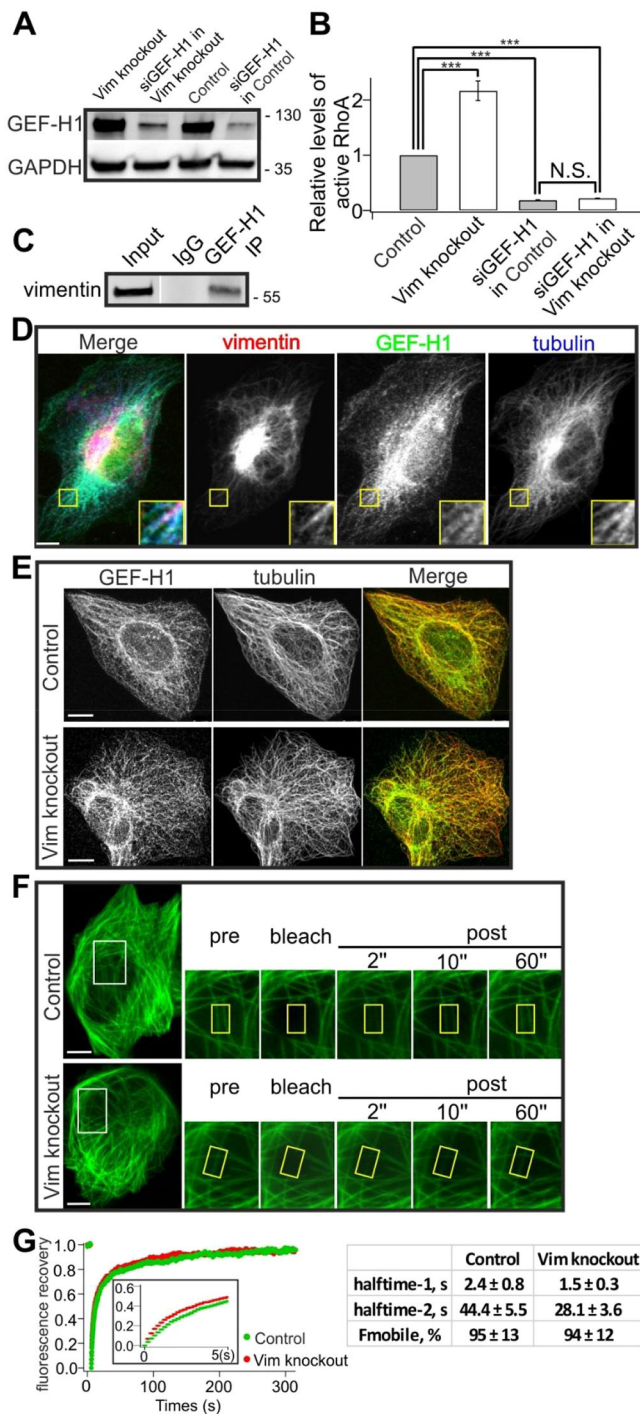


**Fig. 3. Vimentin depletion increases the levels of active RhoA.**

(A) G-LISA analysis of the levels of active RhoA in wild-type, vimentin-knockout, vimentin-knockout-rescue and vimentin overexpression U2OS cells. Data are from five independent experiments and were normalized to control cells.  $*P < 0.05$ ,  $***P < 0.001$  (paired *t*-test). (B) Vimentin depletion does not drastically affect the subcellular localization of RhoA. Representative images show control (indicated by arrows) and vimentin-knockout cells co-cultured on same plates. (C) Western blot analysis of RhoA protein levels in control and vimentin-depleted U2OS cells. The blots were also probed with vimentin antibody to confirm that the vimentin-knockout cell culture is not contaminated by wild-type cells, and with GAPDH antibody to verify equal sample loading. Molecular masses in kilodaltons (kDa) are indicated in the blots. The panel on the right shows the quantified relative levels of RhoA protein normalized to internal control GAPDH from three western blots. (D,E) Expression of dominant negative (DN) RhoA inhibits the increase of Tpm4.2 (D) and P-MLC (E) levels in vimentin-knockout cells. Panels on the left show representative images of DN-RhoA-expressing cells (indicated by arrows) in a vimentin-knockout background. Panels on the right show the quantifications of normalized relative Tpm4.2 (D, 31 control cells from ten images; 25 DN-RhoA expressing cells from ten images) and P-MLC (E, 27 control cells from nine images; 29 DN-RhoA-expressing cells from nine images) fluorescence intensities. Mean intensity values of control and DN-RhoA overexpression cells from each image were used for statistical analysis.  $***P < 0.001$  (paired *t*-test). The data are presented as mean  $\pm$  s.e.m. N.S., not significant. Scale bars: 10  $\mu$ m.



population (halftime 2) of GEF-H1 were more rapid in vimentin-knockout cells (halftimes 1 and 2 of  $\sim 1.5$  s and  $\sim 28$  s, respectively) compared to control cells (halftimes 1 and 2 of  $\sim 2.4$  s and  $\sim 44$  s, respectively), while the sizes of mobile fractions were very similar in both cases (95% and 94%, respectively) (Fig. 4F,G).

#### Vimentin depletion results in increased activity and phosphorylation of GEF-H1

We next examined whether GEF-H1 activity is affected by vimentin. By using an activity assay that is based on co-sedimentation of GEFs with the GST-RhoA-G17A nucleotide-free mutant (Garcia-Mata

**Fig. 4. GEF-H1 is critical for vimentin-mediated suppression of RhoA activity.** (A) Western blot demonstrating that GEF-H1 was efficiently silenced by siRNA (siGEF-H1) in both control and vimentin-knockout cells. The blot was also probed with GAPDH antibody to verify equal sample loading. (B) G-LISA analysis of the levels of active RhoA in GEF-H1-silenced control and vimentin-knockout cells. The data are from five independent experiments and were normalized to results in control cells.  $***P < 0.001$  (paired *t*-test). (C) Co-immunoprecipitation (IP) of GEF-H1 with vimentin from U2OS cell extracts. Whole-cell extracts were used for immunoprecipitation with an anti-GEF-H1 antibody, then probed with an anti-vimentin antibody. IgG is shown as a negative control. Molecular masses in kilodaltons (kDa) are indicated. (D) Image of a cell transfected with vimentin-mCherry, and stained with GEF-H1 and tubulin antibodies. Magnified regions from the area indicated by a yellow box demonstrate that vimentin filaments often colocalize with GEF-H1-containing microtubules. (E) Endogenous GEF-H1 displayed similar colocalization with microtubules in both control and vimentin-knockout cells. (F) Representative examples of GFP-GEF-H1 dynamics in control and vimentin-knockout cells as examined by FRAP. (G) Averaged recovery curves of the raw data are shown on the left (control  $n=15$ ; vimentin knockout,  $n=17$ ). The insert shows the recovery curves during the first 5 s following photobleaching. The averaged curves were fitted with double exponential equation, and mobile fractions and half-time values were calculated from the fitted data. The data are presented as mean  $\pm$  s.e.m. N.S., not significant. Scale bars: 10  $\mu$ m.

et al., 2006), we revealed that the level of active GEF-H1 was  $\sim 3$ -fold higher in vimentin-knockout cells compared to control cells (Fig. 5A). To elucidate the underlying mechanism, we examined the effects of vimentin depletion on phosphorylation of GEF-H1 on Ser886 (which is the only GEF-H1 phosphorylation site for which a commercial antibody is available). The specificity of the antibody was confirmed by western blot in cells expressing phosphorylation-deficient (S886A) GEF-H1 mutant (Fig. S4C). Strikingly, our results showed that GEF-H1 phosphorylation on Ser886 was strongly elevated in vimentin-knockout and knockdown versus control U2OS cells (Fig. 5B, Fig. S4B), whereas GEF-H1 protein and mRNA levels were not significantly altered (Fig. S3E). This mechanism is not specific to the cell type, because knockdown of vimentin from HDF cells resulted in a similar increase in GEF-H1 phosphorylation on Ser886 (Fig. S4A,B).

GEF-H1 phosphorylation on Ser886 was previously shown to induce 14-3-3 binding to the exchange factor, and relocation of 14-3-3 proteins to microtubules (Zenke et al., 2004). To determine whether GEF-H1 phosphorylation on Ser886 regulates the enzymatic activity of GEF-H1 in the context of actin stress fiber assembly, we examined the effects of wild-type GEF-H1 as well as the phosphomimetic (S886D) and phosphorylation-deficient (S886A) GEF-H1 mutants on RhoA activity in U2OS cells by using the G-LISA assay. Because transfection efficiency of these cells is quite high ( $>80\%$ ) for all GEF-H1 constructs, it was possible to examine the effects of these constructs on RhoA-activity using transiently transfected cells. Whereas wild-type GEF-H1-expressing cells displayed only a relatively small increase in the levels of active RhoA compared to control cells expressing GFP, overexpression of the phosphomimetic S886D mutant resulted in an almost 2-fold increase in the levels of active RhoA. The phosphorylation-deficient S886A mutant did not increase active RhoA over control levels (Fig. 5C). Furthermore, expression of the phosphomimetic S886D GEF-H1 resulted in increases in Tpm4.2 and P-MLC levels, whereas expression of the S886A GEF-H1 mutant had no detectable effects on Tpm4.2 or P-MLC levels (Fig. 5D,E). These data show that GEF-H1 phosphorylation on Ser886 increases its guanine nucleotide exchange activity towards RhoA, and consequently affects stress fiber assembly and contractility.

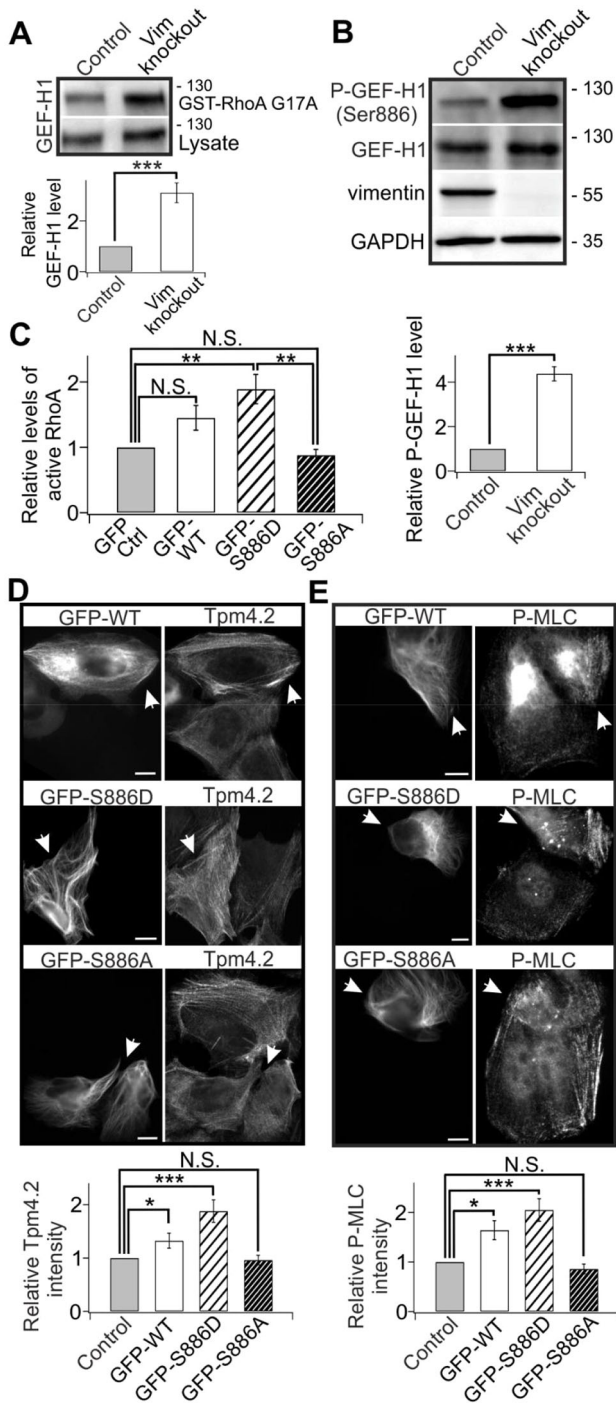


**Fig. 5. Vimentin depletion results in increased activity and phosphorylation of GEF-H1.**

(A) Active GEF-H1 was co-sedimented with GST-RhoA-G17A, and detected by western blotting using an anti-GEF-H1 antibody. The lower panel shows the quantification of normalized relative levels of GEF-H1 co-sedimenting with GST-RhoA-G17A compared to total GEF-H1 levels in cell lysates from five western blots.  $***P < 0.001$  (paired *t*-test). (B) Western blot analysis of GEF-H1 phosphorylated on Ser886 and total GEF-H1 levels in control and vimentin-knockout cells. The blots were also probed with vimentin antibody to confirm that the vimentin-knockout cell culture is not contaminated by wild-type cells, and with GAPDH antibody to verify equal sample loading. The lower panel shows the quantification of normalized relative levels of P-GEF-H1 (Ser886) compared to total GEF-H1 levels from five western blots.  $***P < 0.001$  (paired *t*-test). Molecular masses in kilodaltons (kDa) are indicated. (C) G-LISA analysis of the levels of active RhoA in wild-type, phospho-mimic (S886D) and phospho-deficient (S886A) GEF-H1-expressing cells. The data are from five independent experiments and were normalized to control cells.  $**P < 0.01$  (paired *t*-test). (D) Tpm4.2 levels are increased in cells expressing the phospho-mimic (S886D) GEF-H1 mutant, but not in cells expressing the phospho-deficient (S886A) mutant. Upper panels show representative images of control cells and cells expressing wild-type or mutant GEF-H1 (arrowheads). The lower panel shows the quantification of normalized relative Tpm4.2 fluorescence intensities (wild-type GEF-H1: 32 control cells from nine images and 31 transfected cells from nine images; GEF-H1-S886D: 32 control cells from ten images and 35 transfected cells from total ten images; GEF-H1-S886A: 32 control cells from nine images and 38 transfected cells from nine images). Mean intensity values of control and GEF-H1 overexpression cells from each image were used for statistical analysis.  $*P < 0.05$ ;  $***P < 0.001$  (paired *t*-test). (E) P-MLC levels are increased in cells expressing the phospho-mimic (S886D) GEF-H1 mutant, but not in cells expressing the phospho-deficient (S886A) mutant. Upper panels show representative images of control cells and cells expressing wild-type or mutant GEF-H1 (arrowheads). The lower panel shows the quantification of normalized relative P-MLC fluorescence intensities (wild-type GEF-H1: 35 control cells from nine images and 29 transfected cells from nine images; GEF-H1-S886D: 35 control cells from ten images and 33 transfected cells from ten images; GEF-H1-S886A: 35 control cells from nine images and 28 transfected cells from nine images). Mean intensity values of control and GEF-H1 overexpression cells from each image were used for statistical analysis.  $*P < 0.05$ ,  $***P < 0.001$  (paired *t*-test). The data are presented as mean  $\pm$  s.e.m. N.S., not significant. Scale bars: 10  $\mu$ m.

Earlier studies provided evidence that IFs can affect stress fiber formation through plectin-mediated interactions with focal adhesions. The lack of vimentin or plectin were shown to lead to attenuation of the activities of FAK and its downstream kinases and upregulation of a compensatory feedback loop acting on RhoA (Gregor et al., 2014). FAK and its downstream kinases were, in other studies, demonstrated to regulate RhoA by activating its negative regulators RhoA GTPase-activating proteins (GAPs) (Aikawa et al., 2002; Schober et al., 2007). Based on western blot analysis, we found that neither the total protein levels nor the levels of active FAK and MEK1 and MEK2 (MEK1/2; also known MAP2K1 and MAP2K2, respectively) were drastically affected by

vimentin depletion (Fig. S4D). To examine whether activation of FAK has effects on GEF-H1 phosphorylation on Ser886, or on vimentin-mediated attenuation of stress fiber assembly and contractility in U2OS cells, we used inhibitors of FAK (FAK-14) and its downstream kinases MEK1/2 (U0126), which diminished the levels of active phosphorylated kinases (Fig. S4E). While FAK-14 and U0126 slightly reduced the basal levels of GEF-H1 phosphorylation, neither of them inhibited the GEF-H1 phosphorylation on Ser886 induced by vimentin depletion (Fig. 6A,B). Furthermore, these compounds did not rescue the increased Tpm4.2 and P-MLC levels of vimentin-knockout cells (Fig. 6C,D). Taken together, we demonstrate that vimentin controls RhoA activity and stress fiber assembly through a novel GEF-H1-dependent pathway.

## DISCUSSION

Recent studies have demonstrated that the three cytoskeletal systems, actin filaments, microtubules and IFs, interact with each other, and exhibit interconnected functions in cell migration, morphogenesis and mechano-responsiveness (Huber et al., 2015). However, the mechanisms by which IFs affect the assembly and contractility of actin stress fibers have remained obscure. Here, we reveal that, first, vimentin filaments negatively regulate stress fiber assembly and contractility. Consequently, vimentin depletion results in accumulation of a central stress fiber component Tpm4.2 and increased myosin light chain phosphorylation. Second, vimentin

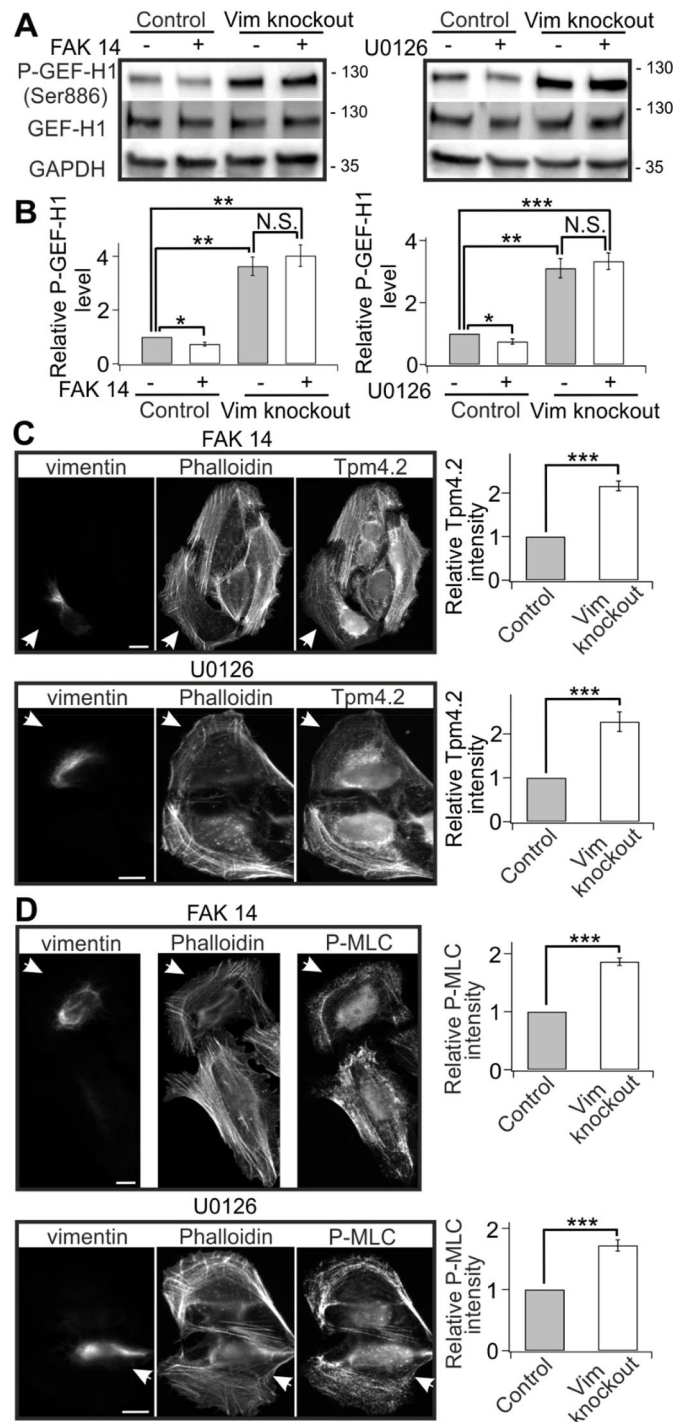


**Fig. 6. GEF-H1 suppression by vimentin does not involve FAK and its downstream kinases.** (A) Western blot analysis of GEF-H1 phosphorylated on Ser886 and total GEF-H1 levels in control and vimentin-depleted U2OS cells incubated in the presence or absence of FAK inhibitor FAK-14 (left panel) or MEK inhibitor U0126 (right panel). The blots were also probed with GAPDH antibodies to verify equal sample loading. Molecular masses in kilodaltons (kDa) are indicated. (B) Quantification of normalized relative levels of P-GEF-H1 (Ser886) compared to total GEF-H1 levels from five western blots for each condition. \* $P < 0.05$ , \*\* $P < 0.01$ , \*\*\* $P < 0.001$  (paired  $t$ -test).

(C,D) Immunostainings demonstrating that neither FAK-14 nor U0126 compounds could suppress the increased Tpm4.2 and P-MLC levels that were induced by depletion of vimentin. Wild-type cells in each panel are indicated with arrowheads. Panels on the right show the quantifications of normalized relative Tpm4.2 (C, FAK14: 28 control cells from six images and 29 vimentin-knockout cells from six images; U0126: 31 control cells from seven images and 28 vimentin-knockout cells from seven images) and P-MLC (D, FAK14: 33 control cells from seven images and 34 vimentin-knockout cells from seven images; U0126: 28 control cells from six images and 27 vimentin-knockout cells from six images) fluorescence intensities. Mean intensity values of control and vimentin-knockout cells from each image were used for statistical analysis. \*\*\* $P < 0.001$  (paired  $t$ -test). The data are presented as mean  $\pm$  s.e.m. N.S., not significant. Scale bars: 10  $\mu$ m.

U2OS cells and dermal fibroblasts, indicating that the pathway by which vimentin regulates actin stress fibers is conserved in different mesenchymal cell types. However, whether the pathway identified here is also conserved in other animal cell types, including epithelial and endothelial cells, remains to be examined. Furthermore, our data provide evidence that Tpm4.2 is unstable in the absence of stress fibers, and thus the elevated Tpm4.2 levels in vimentin-depleted cells are due to increased assembly of stress fibers instead of more direct effects of vimentin, for example on Tpm4.2 transcription. Importantly, the vimentin–GEF-H1–RhoA–stress-fiber pathway identified here is different from the FAK-dependent compensatory feedback loop that was recently proposed to operate in the absence of vimentin and plectin (Gregor et al., 2014). This is because inhibitors against FAK and its downstream kinases could not rescue the effects of vimentin depletion on GEF-H1 phosphorylation, stress fiber assembly and contractility, although they resulted in a small decrease in GEF-H1 phosphorylation levels in control cells. Furthermore, earlier studies proposed that vimentin and plectin depletions regulate RhoA by attenuating the activity of FAK, which in turn leads to downregulation of both ARHGAP35 and ARHGAP5 (also known as p190RhoGAP) (Schober et al., 2007), rather than upregulation of GEF-H1 as shown by our results. Finally, plectin-null cells were shown to exert lower tractions to their environment compared to control cells (Schober et al., 2007; Gregor et al., 2014), whereas our study demonstrates that vimentin depletion increases contractility. Thus, inactivation of plectin and vimentin manifest differently on stress fibers and mechanical regulation of the cell. We do not rule out other mechanisms by which vimentin may control stress fiber assembly, for example, through regulating Rac1 activity via its GEF VAV2 at focal adhesions (Havel et al., 2015). Neither do we rule out other confounding factors including cell density and soft substrates that independently impact vimentin-dependent cell spreading and contractility (Mendez et al., 2014). In this regard, we emphasize that our findings were concordant between cells on glass and 33 kPa substrates.

How does vimentin control the GEF-H1 activity? First, we showed that GEF-H1 localization to microtubules is not drastically altered upon vimentin depletion. Next, by focusing on the GEF-H1 phosphorylation in control and vimentin-knockout cells, we showed that GEF-H1 phosphorylation on Ser886 was significantly increased in vimentin-deficient cells. Although previous studies

filaments inhibit stress fiber assembly and contractility through down-regulating GEF-H1 and RhoA. Finally, vimentin controls GEF-H1 activity through modulating its phosphorylation on Ser886. Taken together, these data unravel new mechanisms by which vimentin IFs regulate the assembly and contractility of actomyosin bundles. Our results on the interplay between vimentin IFs and stress fibers may also explain why elevated expression levels of vimentin correlate with increased invasion and metastasis potential of cancer cells (e.g. Eckes et al., 1998; Mendez et al., 2010).

We show that vimentin depletion has comparable effects on stress fiber assembly, Tpm4.2 levels and GEF-H1 phosphorylation in both

demonstrated that GEF-H1 phosphorylation simultaneously on both Ser886 and Ser959 or only on Ser959 inhibit its activity (Birkenfeld et al., 2007; Yamahashi et al., 2011; Von Thun et al., 2013), our experiments using a phosphomimetic mutant protein provided evidence that GEF-H1 phosphorylation on Ser886 in U2OS cells results in its activation. Various kinases, including PAKs, Aurora A, Cdk1 and PAR1b (also known as MARK2) can inactivate GEF-H1 by phosphorylating inhibitory sites (Birkenfeld et al., 2007; Callow et al., 2005; Yamahashi et al., 2011), whereas extracellular signal-regulated kinase 1 and 2 (ERK1/2, also known as MAPK3 and MAPK1, respectively) phosphorylates GEF-H1 at the activating site Thr678 (Fujishiro et al., 2008; Guilluy et al., 2011a,b). Thus, as with many GEFs, regulation of GEF-H1 is a complex process, involving phosphorylations on several different sites that affect interactions of the protein with other kinases and interaction partners. These interaction partners may further activate GEF-H1 as demonstrated by a recent study in which the bacterial translocation type III secretion effector VopO was shown to bind GEF-H1 and consequently activate the RhoA–ROCK pathway and actin stress fiber formation (Hiyoshi et al., 2015).

The mechanism by which vimentin downregulates phosphorylation of GEF-H1 on Ser886 can either depend on the availability of GEF-H1 for phosphorylation or from activation of a specific kinase in the absence of vimentin. Previous studies demonstrated that PAK1 phosphorylates GEF-H1 on Ser886 (Zenke et al., 2004). PAK1 silencing also attenuates vimentin phosphorylation on Ser56, and vimentin phosphorylation on Ser56 inversely regulates PAK1 activity in smooth muscle cells stimulated by 5-hydroxytryptamine (5-HT; serotonin) (Li et al., 2006). However, whether vimentin can regulate PAK1 and its downstream signaling in non-muscle cells has not been reported. Our western blot analysis indicated that neither PAK1 protein levels nor its activity (as detected by PAK1 phosphorylation on Thr423) were increased by vimentin depletion in U2OS cells. In addition, PAK1 inhibitor (IPA-3) did not affect the levels of Ser886 phosphorylated GEF-H1 in vimentin-knockout cells (Fig. S4F), indicating that PAK1 is not involved and that the signaling cascade in vimentin-mediated GEF-H1 regulation is more complex and is likely to involve other kinases. Moreover, absence of vimentin resulted in a small, but reproducible, increase in the GEF-H1 dynamics (Fig. 4F,G). Therefore, it is also possible that vimentin depletion does not activate specific kinases, but instead makes GEF-H1 more available for these kinases due to its increased dynamics.

Vimentin is a well-characterized biomarker of epithelial–mesenchymal transitions (EMTs). Several studies on multiple tumor types demonstrated that vimentin is specifically expressed in invasive cell lines, but not in stationary cancer cells (Singh et al., 2003; Hu et al., 2004; Wei et al., 2008). Furthermore, absence of vimentin was shown to lead to decreased cell migration speed and directionality (Eckes et al., 1998, 2000). Our work demonstrating effects of vimentin on GEF-H1 and RhoA activity, and downstream stress fiber assembly and contractility, may provide an explanation for these observations. Because extensive stress fibers enhance adhesion and inhibit cell motility, we speculate that upregulation of vimentin stimulates cell migration at least partially through inhibiting stress fiber assembly and contractility. In this context, it is important to note that altered GEF-H1 activity and expression levels have been linked to cancer progression (Cheng et al., 2012; Cullis et al., 2014; Biondini et al., 2015). Thus, in the future it will be interesting to examine how the vimentin–GEF-H1–RhoA pathway identified in our study contributes to the role of vimentin in cell migration and invasion *in vivo*.

## MATERIALS AND METHODS

### Cell culture and transfections

Human osteosarcoma (U2OS) cells and human dermal fibroblasts (HDFs) were maintained as described in Jiu et al. (2015). Vimentin-knockout U2OS cells were generated using CRISPR/Cas9 methods (Jiu et al., 2015). Transient transfections were performed with FuGENE HD transfection reagent (Promega) according to the manufacturer's instructions. Cells were subsequently incubated for 24 h and either fixed with 4% PFA (for GEF-H1 antibody staining, cells were fixed with methanol) or used for FRAP by detaching the cells with trypsin-EDTA and plating them on fibronectin-coated (10 µg/ml) glass-bottomed dishes (MatTek). For siRNA silencing, pre-annealed 3' oligonucleotide duplexes were transfected into cells on 35 mm plates by using Lipofectamine RNAiMAX transfection reagent (Invitrogen) according to the manufacturer's instructions. Cells were incubated for 72 h for efficient depletion of the target proteins. For the cyclohexamide experiment, both wild-type and vimentin-knockout cells were treated with 20 µg/ml cyclohexamide (Sigma) in complete Dulbecco's modified Eagle's medium (DMEM) and harvested at corresponding time points. For the drug experiments, cells were treated with 10 µM blebbistatin (Sigma) for 30 min, 2 µM FAK inhibitor FAK14 (Tocris) for 30 min, 25 µM MEK inhibitor U0126 (Tocris) for 30 min, or 30 µM PAK1 inhibitor IPA-3 (Tocris) for 1 h before they were harvested for western blot analysis or fixed for immunofluorescence.

### Plasmids and siRNA oligonucleotides

Cloning strategy for constructs expressing GFP-tagged full-length vimentin or 'unit length filament' (ULF) and vimentin–mCherry are described in Yoon et al. (1998) and Eriksson et al. (2004). Dominant negative pRK5myc RhoA N19 (deposited by Alan Hall, Addgene plasmids #15900 and #15901). Wild-type GFP-GEF-H1, phosphomimetic S886D GFP-GEF-H1 and phosphorylation-deficient S886A GFP-GEF-H1 were kind gifts from Katalin Szaszi (St. Michael's Hospital, Toronto, Canada). pGEX-4T1-RhoA G17A was a gift from Rafael Garcia-Mata (Addgene plasmid # 69357). The ON-TARGET siRNA-SMART pool L-003551-00-0005 was used for vimentin knockdown in HDF cells and the siRNA target sequence 5'-UCACGAUGACCUUGAAUAA-3' was used for vimentin knockdown in U2OS and HDF cells (Dharmacon). The siRNA target sequences 5'-GACUCAGACUCUAGCCAGA-3' and 5'-CAGAUGUGUAGACC-UACU-3' were used for GEF-H1 knockdown (Bioneer). AllStars Negative Control siRNA (Qiagen) was used as a control siRNA.

### Western blotting

Cells were washed three times with cold PBS, scraped, and lysed in Laemmli sample buffer (LSB) with 0.3 mM PMSF and protease and phosphatase inhibitor cocktail (Pierce). Protein concentrations were measured by using Bradford reagent (Sigma-Aldrich). 5% milk was used in blocking and washes were done by using TBST buffer (Tris-buffered saline, 0.1% Tween 20). Antibodies were used with the following dilutions in 5% BSA: vimentin rabbit polyclonal D21H3 antibody (dilution 1:1000; #5741, Cell Signaling); Tpm4.2 mouse monoclonal LC24 antibody (dilution 1:500; a kind gift from Peter W. Gunning, UNSW Australia); phospho-myosin light chain 2 (Thr18/Ser19) rabbit polyclonal antibody (dilution 1:500; #3674, Cell Signaling); myosin light chain mouse monoclonal antibody (dilution 1:1000; #M4401, Sigma); GEF-H1 rabbit monoclonal 55B6 antibody (dilution 1:1000; #4076, Cell Signaling); phospho-GEF-H1 (Ser886) rabbit monoclonal E1L6D antibody (dilution 1:1000; #14143, Cell Signaling); actin mouse polyclonal AC40 antibody (dilution 1:1000; #A4700, Sigma); RhoA rabbit polyclonal antibody (dilution 1:1000; #SAB2102002, Sigma); FAK rabbit polyclonal antibody (dilution 1:1000; #3285, Cell Signaling); phospho-FAK (Tyr397) rabbit polyclonal antibody (dilution 1:1000; #3283, Cell Signaling); MEK1/2 mouse polyclonal L38C12 antibody (dilution 1:1000; #4694, Cell Signaling); phospho-MEK1/2 (Ser217/221) rabbit polyclonal 41G9 antibody (dilution 1:1000; #9154, Cell Signaling); PAK1 rabbit polyclonal antibody (dilution 1:1000; #2602, Cell Signaling); phospho-PAK1 (Thr423) rabbit polyclonal antibody (dilution 1:1000; #2601, Cell Signaling); GAPDH mouse polyclonal antibody (dilution 1:1000; G8795, Sigma). Horseradish peroxidase (HRP)-linked secondary antibodies were used and chemiluminescence was measured after applying



western blotting ECL spray (Advansta). The ImageJ program was applied to measure the band intensities of blots. In the quantifications, we calculated the intensity ratios of phosphorylated protein to protein of interest versus total protein to the internal control GAPDH. The values of control cells were set to 1 in each experiment, and the differences between the control and the knockout, knockdown or drug treatment cells in corresponding blots were calculated. The statistical differences between the two groups were assessed using the paired *t*-test.  $P < 0.05$  was considered significant.

### Immunofluorescence microscopy

Immunofluorescence experiments were performed as previously described (Jiu et al., 2015). Briefly, the cells were fixed with 4% PFA, washed three times with 0.2% BSA in Dulbecco's phosphate buffered saline and permeabilized with 0.1% Triton X-100 in PBS. The following primary antibodies were used: vimentin rabbit polyclonal D21H3 antibody (dilution 1:100; #5741, Cell Signaling) when cells were co-stained with Tpm4.2 antibody; vimentin mouse polyclonal V9 antibody (dilution 1:100; #V6630, Sigma) when cells were co-stained with P-MLC antibody; Tpm4.2 mouse monoclonal LC24 antibody (dilution 1:150; a kind gift from Peter W. Gunning, UNSW Australia); phospho-myosin light chain 2 (Thr18/Ser19) rabbit polyclonal antibody (dilution 1:100; #3674, Cell Signaling); RhoA rabbit polyclonal antibody (dilution 1:100; #SAB2102002, Sigma); GEF-H1 rabbit polyclonal antibody (dilution 1:50; #ab155785, Abcam); tubulin mouse monoclonal antibody (dilution 1:100; #4026, Sigma). Secondary antibodies were conjugated to Alexa Fluor 488, 568 or 647 (Invitrogen). F-actin was visualized with Alexa Fluor 488-, 568- or 647 conjugated to phalloidin (dilution 1:200; Invitrogen). Cells were imaged either with a wide-field fluorescence microscope (Leica DM6000) with a HCXPL APO 63×1.40–0.60 NA oil objective or by Leica TCS SP5 laser scanning confocal microscope with a 63×1.3 NA glycerol objective. Because the GEF-H1 antibody from Cell Signaling used for all western blot experiments does not work in immunofluorescence, we used GEF-H1 antibody from Abcam for immunofluorescence experiments where cells were fixed by methanol for 5 min at  $-20^{\circ}\text{C}$ . For comparing Tpm4.2, P-MLC and RhoA levels, the control and vimentin-knockout or knockdown cells were mixed and distinguished from each other by vimentin antibody staining. Please note that vimentin, Tpm4.2, P-MLC, RhoA and GEF-H1 levels were constant between different control cells (data not shown). In the quantifications, we first measured the intensities (corresponding to expression levels) of a protein of interest in all control cells from individual immunofluorescence images and set the mean value to 1. Subsequently, the values from all knockout or knockdown cells from the same image were compared to the mean value obtained from the control cells. The mean intensity values of knockout or knockdown cells (normalized to the values obtained from control cells) from individual immunofluorescence images were used for the statistical analysis. s.e.m. represents the variation of mean intensities between individual immunofluorescence images. The statistical differences between two groups was assessed by using a paired *t*-test.  $P < 0.05$  was considered significant.

### FRAP

To analyze the kinetics of GEF-H1, wild-type and vimentin-knockout cells were transfected with GFP-GEF-H1 and incubated for 24 h. Confocal images were acquired with a 3I Marianas imaging system (3I Intelligent Imaging Innovations), consisting of an inverted spinning disk confocal microscope Zeiss Axio Observer Z1 (Zeiss), a Yokogawa CSU-X1 M1 confocal scanner and 63×1.2 NA WC-Apochromat Corr WD=0.28 M27 objective (Zeiss). A heated sample environment ( $+37^{\circ}\text{C}$ ) and  $\text{CO}_2$  control were used. SlideBook 6.0 software (3I Intelligent Imaging Innovations) was used for the image acquisition. Five pre-bleach images were acquired followed by bleaching scans with 100% intensity laser lines over the region of interest. Recovery of fluorescence was monitored 50 times every 200 ms and 300 times every 1 s. The intensity of the bleached area was normalized to a neighboring non-bleached area. Mean scatter plots were calculated from different FRAP experiments and the data were fitted with SigmaPlot 11.0 to  $f = a \times (1 - \exp(-b \times x)) + c \times (1 - \exp(-d \times x))$  double exponential equations. Recovery halftimes were obtained for each recovery curve and the means and standard deviations were calculated.

### Quantitative real-time RT-PCR

The total RNA was extracted from U2OS cells using RNeasy mini kits (Qiagen). cDNA was obtained by reverse-transcribing the same amount of total RNA using High Capacity cDNA Reverse Transcription Kit (Applied Biosystems). The complementary DNA products were amplified using sequence-specific primers for Tpm4.2 (forward, 5'-AGA-AAGCGCTGAGGACAAG-3'; reverse, 5'-TTGGTGAGCCCTGTCCAACT-3'), RhoA (forward, 5'-CATCCGCTCCTTTGATGATCTT-3'; reverse, 5'-TGCTCGGGTCATGTTCAAGT-3'), GEF-H1 (forward, 5'-AGCCTGTGGAAAGACATGCTT-3'; reverse, 5'-TCAAACACTGTGGGCACATAC-3') and GAPDH (forward, 5'-TCGGTGTGAACGGATTG-3'; reverse, 5'-GGTCTCGCTCCTGGAAGA-3'). The transcript levels of the genes of interest were measured by qRT-PCR using the SYBR Green PCR mix (Applied Biosystems) in an Applied Biosystems 7300 detection system (Bio-Rad). The data were normalized to the expression levels of the cellular housekeeping gene GAPDH.

### RhoA activity assay

RhoA activity was measured by using a RhoA G-LISA absorbance-based biochemical assay kit (Cytoskeleton) according to the manufacturer's instructions. In brief, cells were lysed, aliquoted and snap frozen in liquid nitrogen. After rapid thawing, binding buffer was added to the cell lysate, which was subsequently incubated on a RhoA-GTP affinity plate coated with RhoA-GTP-binding protein in each well. The plate was placed on an orbital plate shaker at 400 rpm for 30 min at  $4^{\circ}\text{C}$ . After washes, primary anti-RhoA antibodies (1:250) and secondary HRP-linked antibodies (1:62.5) were sequentially added to the wells followed by an incubation on an orbital shaker at 400 rpm for 45 min at room temperature. Thereafter, the signal was developed with HRP-detection reagents. The absorbance was measured by means of a plate reader spectrophotometer Enspire (PerkinElmer). In the quantifications, the absorbance values of control cells were set to 1 in each experiment, and the differences between the control and the knockout, knockdown or transfection cells in corresponding experiments were calculated. The statistical differences between the two groups were assessed using the paired *t*-test.  $P < 0.05$  was considered significant.

### GEF activity assay

The activity of GEF-H1 was assayed by using GST-RhoA-G17A nucleotide-free mutants as described previously (Garcia-Mata et al., 2006). Cells were lysed in lysis buffer (150 mM NaCl, 20 mM HEPES, pH 7.4, 5 mM  $\text{MgCl}_2$ , 1% Triton X-100, 1 mM DTT, 1 mM PMSF, 10  $\mu\text{g}/\text{ml}$  aprotinin and leupeptin), incubated with 50  $\mu\text{g}/\text{ml}$  glutathione-Sepharose-bound GST-RhoA G17A for 60 min at  $4^{\circ}\text{C}$ , and washed in the lysis buffer. Samples were subsequently analyzed by western blotting with the GEF-H1 antibody.

### Co-immunoprecipitation

Cells were harvested and lysed in NP-40 lysis buffer (50 mM Tris-HCl pH 7.4, 50 mM NaCl, 0.1% Triton X-100, 1% NP-40) plus 1× Roche complete protease inhibitors (Roche). Total cell lysate was used for immunoprecipitation. Primary GEF-H1 antibody (10  $\mu\text{g}$ ) was incubated with 50  $\mu\text{l}$  (1.5 mg) of Dynabeads (Life Technologies) for 2 h at  $4^{\circ}\text{C}$  while under rotating. Cell lysate was then mixed with Dynabeads-antibody complexes and incubated overnight at  $4^{\circ}\text{C}$  while under rotating. After three 20 min washes with NP-40 lysis buffer, the protein-antibody complexes were eluted from the beads in 20  $\mu\text{l}$  NuPAGE LDS sample buffer. Samples were subsequently analyzed by western blotting with the vimentin antibody.

### Polyacrylamide substrate preparation

Polyacrylamide (PA) gels were constructed and coated with fibronectin as described previously (Damjanovic et al., 2005). Briefly, coverslips were treated with 3-aminopropyltrimethoxy silane, dried and soaked in 0.5% glutaraldehyde. In order to prepare gels of 33 kPa stiffness, acrylamide (40%, Bio-Rad), Bis (2%, Bio-Rad), HEPES (1 M) and distilled water were mixed in concentrations of 5% acrylamide with 0.12% Bis. Gels were crosslinked using ammonium persulfate (10%) and TEMED. A 15  $\mu\text{l}$  of the mixture was allowed to polymerize between the activated coverslip and a

normal coverslip. PA gels needed for the experiments were constructed concurrently and used immediately. PA gels were activated for protein cross-linking with sulfo-SANPAH (Pierce Biotechnology) under a UV lamp and coated with fibronectin (10 µg/ml) at 4°C overnight. Prior to experiments, the gels were covered with PBS in UV lamp for 30 min to sterilize and then equilibrated with DMEM at 4°C, 5% CO<sub>2</sub>, for 45 min.

### Traction force microscopy

Both control and vimentin-knockout cells were cultured for 3–8 h on custom-made 35 mm dishes (Matrigen) with fibronectin-coated polyacrylamide gel (elastic modulus 25 kPa). 200 nm YG fluorescent (505/515) microspheres were immobilized to the surface of the gel as described previously (Marinkovic et al., 2012). Using an inverted fluorescence microscope (31 Marianas), images of the cells and of the fluorescent microspheres directly underneath the cells were acquired during the experiments and after cell detachment with trypsin. By comparing the reference image with the experimental image, we computed the cell-exerted displacement field. From the displacement fields, and manual traces of the cell contours, together with knowledge of substrate stiffness, we computed the traction force fields using the approach of constrained Fourier-transform traction cytometry (Butler et al., 2002). From the traction fields, we calculated the root mean squared values (RMS) of tractions. Because tractions vary log-normally (Krishnan et al., 2009), statistical differences in RMS traction between the control and vimentin-knockout groups were assessed by using the Mann–Whitney–Wilcoxon rank-sum (MWW) test.  $P < 0.05$  was considered significant.

### Competing interests

The authors declare no competing or financial interests.

### Author contributions

Y.J. performed majority of the experiments, data analysis, and interpretation of the data. N.S. and R.K. performed the traction force data analysis. F.C. participated in qRT-PCR experiments. Y.J., J.P., J.E.E., R.K. and P.L. participated in designing of the study and wrote the manuscript.

### Funding

This study was supported by grants from the Suomen Akatemia (Academy of Finland) (274565 to Y.J.), Jane ja Aatos Erkon Säätiö (Jane and Aatos Erkkö Foundation), and the Sigrid Juséliuksen Säätiö (Sigrid Juselius Foundation) (to P.L.). This study was also supported by a grant from the National Institutes of Health (R21HL123522 to R.K. and N.S.). Deposited in PMC for immediate release.

### Supplementary information

Supplementary information available online at <http://jcs.biologists.org/lookup/doi/10.1242/jcs.196881.supplemental>

### References

- Abrahamsberg, C., Fuchs, P., Osmanagic-Myers, S., Fischer, I., Propst, F., Elbe-Burger, A. and Wiche, G. (2005). Targeted ablation of plectin isoform 1 uncovers role of cytolinker proteins in leukocyte recruitment. *Proc. Natl. Acad. Sci. USA* **102**, 18449–18454.
- Aikawa, R., Nagai, T., Kudoh, S., Zou, Y., Tanaka, M., Tamura, M., Akazawa, H., Takano, H., Nagai, R. and Komuro, I. (2002). Integrins play a critical role in mechanical stress-induced p38 MAPK activation. *Hypertension* **39**, 233–238.
- Andra, K., Nikolic, B., Stocher, M., Drenckhahn, D. and Wiche, G. (1998). Not just scaffolding: plectin regulates actin dynamics in cultured cells. *Genes Dev.* **12**, 3442–3451.
- Bhattacharya, R., Gonzalez, A. M., DeBiase, P. J., Trejo, H. E., Goldman, R. D., Flitney, F. W. and Jones, J. C. R. (2009). Recruitment of vimentin to the cell surface by beta3 integrin and plectin mediates adhesion strength. *J. Cell Sci.* **122**, 1390–1400.
- Biondini, M., Duclos, G., Meyer-Schaller, N., Silberzan, P., Camonis, J. and Parrini, M. C. (2015). RalB regulates contractility-driven cancer dissemination upon TGFbeta stimulation via the RhoGEF GEF-H1. *Sci. Rep.* **5**, 11759.
- Birkenfeld, J., Nalbant, P., Bohl, B. P., Pertz, O., Hahn, K. M. and Bokoch, G. M. (2007). GEF-H1 modulates localized RhoA activation during cytokinesis under the control of mitotic kinases. *Dev. Cell* **12**, 699–712.
- Burnette, D. T., Manley, S., Sengupta, P., Sougrat, R., Davidson, M. W., Kachar, B. and Lippincott-Schwartz, J. (2011). A role for actin arcs in the leading-edge advance of migrating cells. *Nat. Cell Biol.* **13**, 371–382.
- Burridge, K. and Wittchen, E. S. (2013). The tension mounts: stress fibers as force-generating mechanotransducers. *J. Cell Biol.* **200**, 9–19.
- Butler, J. P., Tolic-Norrelykke, I. M., Fabry, B. and Fredberg, J. J. (2002). Traction fields, moments, and strain energy that cells exert on their surroundings. *Am. J. Physiol. Cell Physiol.* **282**, C595–C605.
- Callow, M. G., Zozulya, S., Gishizky, M. L., Jallal, B. and Smeal, T. (2005). PAK4 mediates morphological changes through the regulation of GEF-H1. *J. Cell Sci.* **118**, 1861–1872.
- Cheng, I. K. C., Tsang, B. C. K., Lai, K. P., Ching, A. K. K., Chan, A. W. H., To, K. F., Lai, P. B. S. and Wong, N. (2012). GEF-H1 over-expression in hepatocellular carcinoma promotes cell motility via activation of RhoA signaling. *J. Pathol.* **228**, 575–585.
- Cullis, J., Meiri, D., Sandi, M. J., Radulovich, N., Kent, O. A., Medrano, M., Mokady, D., Normand, J., Larose, J., Marcotte, R. et al. (2014). The RhoGEF GEF-H1 is required for oncogenic RAS signaling via KSR-1. *Cancer Cell* **25**, 181–195.
- Damljanovic, V., Lagerholm, B. C. and Jacobson, K. (2005). Bulk and micropatterned conjugation of extracellular matrix proteins to characterized polyacrylamide substrates for cell mechanotransduction assays. *Biotechniques* **39**, 847–851.
- Dupin, I., Sakamoto, Y. and Etienne-Manneville, S. (2011). Cytoplasmic intermediate filaments mediate actin-driven positioning of the nucleus. *J. Cell Sci.* **124**, 865–872.
- Eckes, B., Dogic, D., Colucci-Guyon, E., Wang, N., Maniotis, A., Ingber, D., Merckling, A., Langa, F., Aumailley, M., Delouee, A. et al. (1998). Impaired mechanical stability, migration and contractile capacity in vimentin-deficient fibroblasts. *J. Cell Sci.* **111**, 1897–1907.
- Eckes, B., Colucci-Guyon, E., Smola, H., Nodder, S., Babinet, C., Krieg, T. and Martin, P. (2000). Impaired wound healing in embryonic and adult mice lacking vimentin. *J. Cell Sci.* **113**, 2455–2462.
- Eriksson, J. E., He, T., Trejo-Skalli, A. V., Harmala-Brasken, A.-S., Hellman, J., Chou, Y.-H. and Goldman, R. D. (2004). Specific in vivo phosphorylation sites determine the assembly dynamics of vimentin intermediate filaments. *J. Cell Sci.* **117**, 919–932.
- Eriksson, J. E., Dechat, T., Grin, B., Helfand, B., Mendez, M., Pallari, H.-M. and Goldman, R. D. (2009). Introducing intermediate filaments: from discovery to disease. *J. Clin. Invest.* **119**, 1763–1771.
- Esue, O., Carson, A. A., Tseng, Y. and Wirtz, D. (2006). A direct interaction between actin and vimentin filaments mediated by the tail domain of vimentin. *J. Biol. Chem.* **281**, 30393–30399.
- Fujishiro, S.-H., Tanimura, S., Mure, S., Kashimoto, Y., Watanabe, K. and Kohno, M. (2008). ERK1/2 phosphorylate GEF-H1 to enhance its guanine nucleotide exchange activity toward RhoA. *Biochem. Biophys. Res. Commun.* **368**, 162–167.
- Fujiwara, S., Ohashi, K., Mashiko, T., Kondo, H. and Mizuno, K. (2016). Interplay between Solo and keratin filaments is crucial for mechanical force-induced stress fiber reinforcement. *Mol. Biol. Cell* **27**, 954–966.
- Garcia-Mata, R., Wennerberg, K., Arthur, W. T., Noren, N. K., Ellerbroek, S. M. and Burridge, K. (2006). Analysis of activated GAPs and GEFs in cell lysates. *Methods Enzymol.* **406**, 425–437.
- Geeves, M. A., Hitchcock-DeGregori, S. E. and Gunning, P. W. (2015). A systematic nomenclature for mammalian tropomyosin isoforms. *J. Muscle Res. Cell Motil.* **36**, 147–153.
- Gregor, M., Osmanagic-Myers, S., Burgstaller, G., Wolfram, M., Fischer, I., Walko, G., Resch, G. P., Jorgl, A., Herrmann, H. and Wiche, G. (2014). Mechanosensing through focal adhesion-anchored intermediate filaments. *FASEB J.* **28**, 715–729.
- Guilluy, C., Dubash, A. D. and Garcia-Mata, R. (2011a). Analysis of RhoA and Rho GEF activity in whole cells and the cell nucleus. *Nat. Protoc.* **6**, 2050–2060.
- Guilluy, C., Swaminathan, V., Garcia-Mata, R., O'Brien, E. T., Superfine, R. and Burridge, K. (2011b). The Rho GEFs LARG and GEF-H1 regulate the mechanical response to force on integrins. *Nat. Cell Biol.* **13**, 724–729.
- Havel, L. S., Kline, E. R., Salgueiro, A. M. and Marcus, A. I. (2015). Vimentin regulates lung cancer cell adhesion through a VAV2-Rac1 pathway to control focal adhesion kinase activity. *Oncogene* **34**, 1979–1990.
- Heasman, S. J. and Ridley, A. J. (2008). Mammalian Rho GTPases: new insights into their functions from in vivo studies. *Nat. Rev. Mol. Cell Biol.* **9**, 690–701.
- Hiyoshi, H., Okada, R., Matsuda, S., Gotoh, K., Akeda, Y., Iida, T. and Kodama, T. (2015). Interaction between the type III effector VopO and GEF-H1 activates the RhoA-ROCK pathway. *PLoS Pathog.* **11**, e1004694.
- Hollenbeck, P. J., Bershady, A. D., Pletjushkina, O. Y., Tint, I. S. and Vasiliev, J. M. (1989). Intermediate filament collapse is an ATP-dependent and actin-dependent process. *J. Cell Sci.* **92**, 621–631.
- Hotulainen, P. and Lappalainen, P. (2006). Stress fibers are generated by two distinct actin assembly mechanisms in motile cells. *J. Cell Biol.* **173**, 383–394.
- Hu, L., Lau, S. H., Tzang, C. H., Wen, J. M., Wang, W., Xie, D., Huang, M., Wang, Y., Wu, M. C., Huang, J. F. et al. (2004). Association of Vimentin overexpression and hepatocellular carcinoma metastasis. *Oncogene* **23**, 298–302.
- Huber, F., Boire, A., López, M. P. and Koenderink, G. H. (2015). Cytoskeletal crosstalk: when three different personalities team up. *Curr. Opin. Cell Biol.* **32**, 39–47.

- Jiu, Y., Lehtimäki, J., Tojkander, S., Cheng, F., Jääliñoja, H., Liu, X., Varjosalo, M., Eriksson, J. E. and Lappalainen, P. (2015). Bidirectional Interplay between Vimentin Intermediate Filaments and Contractile Actin Stress Fibers. *Cell Rep.* **11**, 1511-1518.
- Krendel, M., Zenke, F. T. and Bokoch, G. M. (2002). Nucleotide exchange factor GEF-H1 mediates cross-talk between microtubules and the actin cytoskeleton. *Nat. Cell Biol.* **4**, 294-301.
- Krishnan, R., Park, C. Y., Lin, Y.-C., Mead, J., Jaspers, R. T., Trepatt, X., Lenormand, G., Tambe, D., Smolensky, A. V., Knoll, A. H. et al. (2009). Reinforcement versus fluidization in cytoskeletal mechanoresponsiveness. *PLoS ONE* **4**, e5486.
- Leduc, C. and Etienne-Manneville, S. (2015). Intermediate filaments in cell migration and invasion: the unusual suspects. *Curr. Opin. Cell Biol.* **32**, 102-112.
- Lessey, E. C., Guilluy, C. and Burridge, K. (2012). From mechanical force to RhoA activation. *Biochemistry* **51**, 7420-7432.
- Li, Q.-F., Spinelli, A. M., Wang, R., Anfinogenova, Y., Singer, H. A. and Tang, D. D. (2006). Critical role of vimentin phosphorylation at Ser-56 by p21-activated kinase in vimentin cytoskeleton signaling. *J. Biol. Chem.* **281**, 34716-34724.
- Loschke, F., Seltmann, K., Bouameur, J.-E. and Magin, T. M. (2015). Regulation of keratin network organization. *Curr. Opin. Cell Biol.* **32**, 56-64.
- Marinkovic, A., Mih, J. D., Park, J.-A., Liu, F. and Tschumperlin, D. J. (2012). Improved throughput traction microscopy reveals pivotal role for matrix stiffness in fibroblast contractility and TGF-beta responsiveness. *Am. J. Physiol. Lung Cell Mol. Physiol.* **303**, L169-L180.
- Mathews, H. K., Delabre, U., Rohn, J. L., Guck, J., Kunda, P. and Baum, B. (2012). Changes in Ect2 localization couple actomyosin-dependent cell shape changes to mitotic progression. *Dev. Cell* **23**, 371-383.
- Meier, M., Padilla, G. P., Herrmann, H., Wedig, T., Hergt, M., Patel, T. R., Stetefeld, J., Aebi, U. and Burkhard, P. (2009). Vimentin coil 1A-A molecular switch involved in the initiation of filament elongation. *J. Mol. Biol.* **390**, 245-261.
- Mendez, M. G., Kojima, S. I. and Goldman, R. D. (2010). Vimentin induces changes in cell shape, motility, and adhesion during the epithelial to mesenchymal transition. *FASEB J.* **24**, 1838-1851.
- Mendez, M. G., Restle, D. and Janmey, P. A. (2014). Vimentin enhances cell elastic behavior and protects against compressive stress. *Biophys. J.* **107**, 314-323.
- Nalbant, P., Chang, Y.-C., Birkenfeld, J., Chang, Z.-F. and Bokoch, G. M. (2009). Guanine nucleotide exchange factor-H1 regulates cell migration via localized activation of RhoA at the leading edge. *Mol. Biol. Cell* **20**, 4070-4082.
- Pathak, R., Delorme-Walker, V. D., Howell, M. C., Anselmo, A. N., White, M. A., Bokoch, G. M. and DerMardirossian, C. (2012). The microtubule-associated Rho activating factor GEF-H1 interacts with exocyst complex to regulate vesicle traffic. *Dev. Cell* **23**, 397-411.
- Ren, Y., Li, R., Zheng, Y. and Busch, H. (1998). Cloning and characterization of GEF-H1, a microtubule-associated guanine nucleotide exchange factor for Rac and Rho GTPases. *J. Biol. Chem.* **273**, 34954-34960.
- Sanger, J. W., Kang, S., Siebrands, C. C., Freeman, N., Du, A., Wang, J., Stout, A. L. and Sanger, J. M. (2005). How to build a myofibril. *J. Muscle. Res. Cell Motil.* **26**, 343-354.
- Schober, M., Raghavan, S., Nikolova, M., Polak, L., Pasolli, H. A., Beggs, H. E., Reichardt, L. F. and Fuchs, E. (2007). Focal adhesion kinase modulates tension signaling to control actin and focal adhesion dynamics. *J. Cell Biol.* **176**, 667-680.
- Singh, S., Sadacharan, S., Su, S., Belledegrun, A., Persad, S. and Singh, G. (2003). Overexpression of vimentin: role in the invasive phenotype in an androgen-independent model of prostate cancer. *Cancer Res.* **63**, 2306-2311.
- Skau, C. T., Plotnikov, S. V., Doyle, A. D. and Waterman, C. M. (2015). Inverted formin 2 in focal adhesions promotes dorsal stress fiber and fibrillar adhesion formation to drive extracellular matrix assembly. *Proc. Natl. Acad. Sci. USA* **112**, E2447-E2456.
- Snider, N. T. and Omary, M. B. (2014). Post-translational modifications of intermediate filament proteins: mechanisms and functions. *Nat. Rev. Mol. Cell Biol.* **15**, 163-177.
- Svitkina, T. M., Verkhovsky, A. B. and Borisy, G. G. (1996). Plectin sidearms mediate interaction of intermediate filaments with microtubules and other components of the cytoskeleton. *J. Cell Biol.* **135**, 991-1007.
- Tee, Y. H., Shemesh, T., Thiagarajan, V., Hariadi, R. F., Anderson, K. L., Page, C., Volkmann, N., Hanein, D., Sivaramakrishnan, S., Kozlov, M. M. et al. (2015). Cellular chirality arising from the self-organization of the actin cytoskeleton. *Nat. Cell Biol.* **17**, 445-457.
- Tojkander, S., Gateva, G., Schevzov, G., Hotulainen, P., Naumanen, P., Martin, C., Gunning, P. W. and Lappalainen, P. (2011). A molecular pathway for myosin II recruitment to stress fibers. *Curr. Biol.* **21**, 539-550.
- Tojkander, S., Gateva, G. and Lappalainen, P. (2012). Actin stress fibers—assembly, dynamics and biological roles. *J. Cell Sci.* **125**, 1855-1864.
- Tojkander, S., Gateva, G., Husain, A., Krishnan, R. and Lappalainen, P. (2015). Generation of contractile actomyosin bundles depends on mechanosensitive actin filament assembly and disassembly. *Elife* **4**, e06126.
- von Thun, A., Preisinger, C., Rath, O., Schwarz, J. P., Ward, C., Monsefi, N., Rodríguez, J., Garcia-Munoz, A., Birtwistle, M., Bienvenut, W. et al. (2013). Extracellular signal-regulated kinase regulates RhoA activation and tumor cell plasticity by inhibiting guanine exchange factor H1 activity. *Mol. Cell. Biol.* **33**, 4526-4537.
- Wei, J., Xu, G., Wu, M., Zhang, Y., Li, Q., Liu, P., Zhu, T., Song, A., Zhao, L., Han, Z. et al. (2008). Overexpression of vimentin contributes to prostate cancer invasion and metastasis via src regulation. *Anticancer. Res.* **28**, 327-334.
- Wong, A. J., Pollard, T. D. and Herman, I. M. (1983). Actin filament stress fibers in vascular endothelial cells in vivo. *Science* **219**, 867-869.
- Yamashita, Y., Saito, Y., Murata-Kamiya, N. and Hatakeyama, M. (2011). Polarity-regulating kinase partitioning-defective 1b (PAR1b) phosphorylates guanine nucleotide exchange factor H1 (GEF-H1) to regulate RhoA-dependent actin cytoskeletal reorganization. *J. Biol. Chem.* **286**, 44576-44584.
- Yi, J., Wu, X. S., Crites, T. and Hammer, J. A. III. (2012). Actin retrograde flow and actomyosin II arc contraction drive receptor cluster dynamics at the immunological synapse in Jurkat T cells. *Mol. Biol. Cell* **23**, 834-852.
- Yoon, M., Moir, R. D., Prahlad, V. and Goldman, R. D. (1998). Motile properties of vimentin intermediate filament networks in living cells. *J. Cell Biol.* **143**, 147-157.
- Zenke, F. T., Krendel, M., DerMardirossian, C., King, C. C., Bohl, B. P. and Bokoch, G. M. (2004). p21-activated kinase 1 phosphorylates and regulates 14-3-3 binding to GEF-H1, a microtubule-localized Rho exchange factor. *J. Biol. Chem.* **279**, 18392-18400.

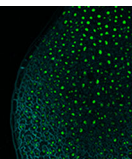
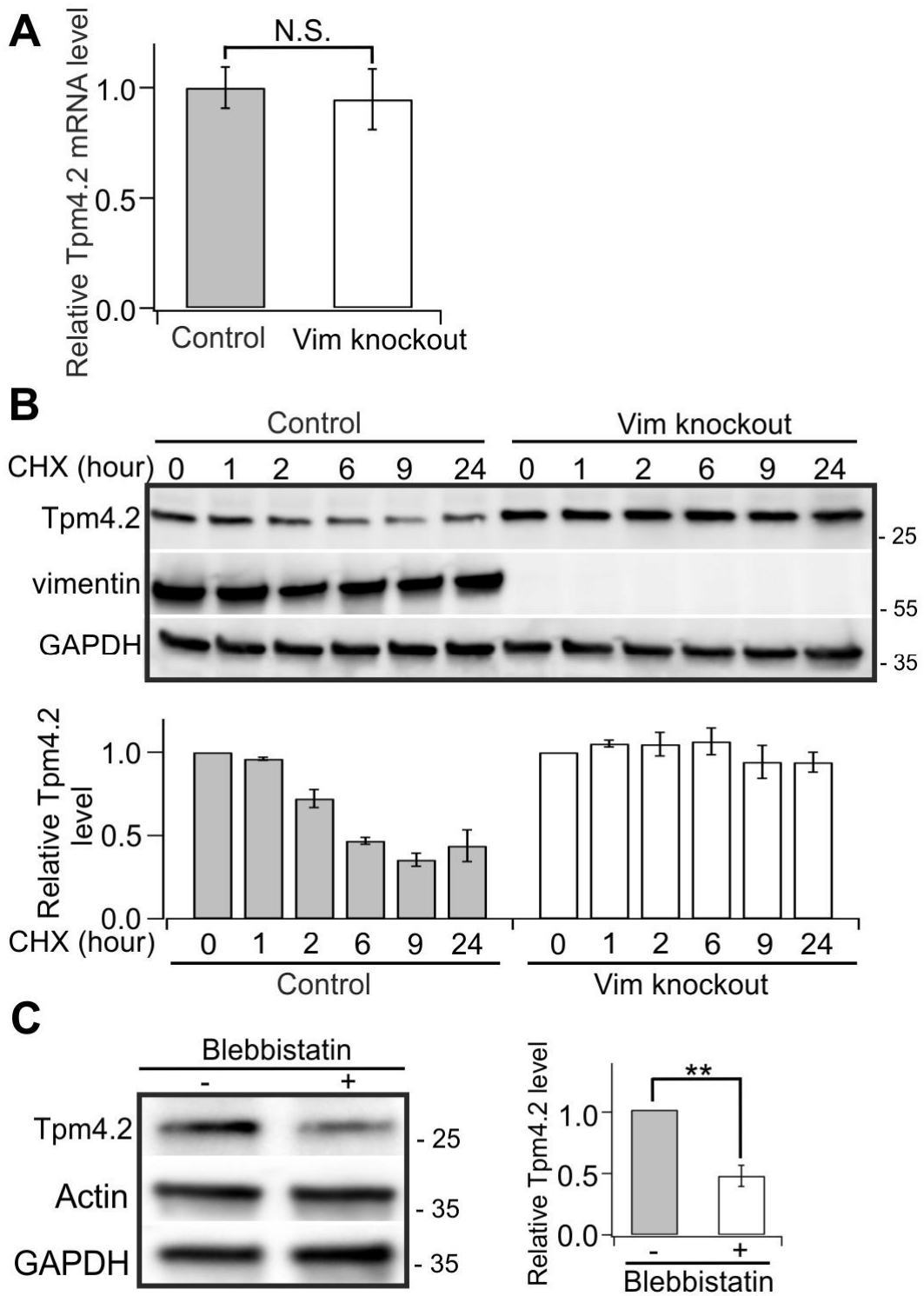
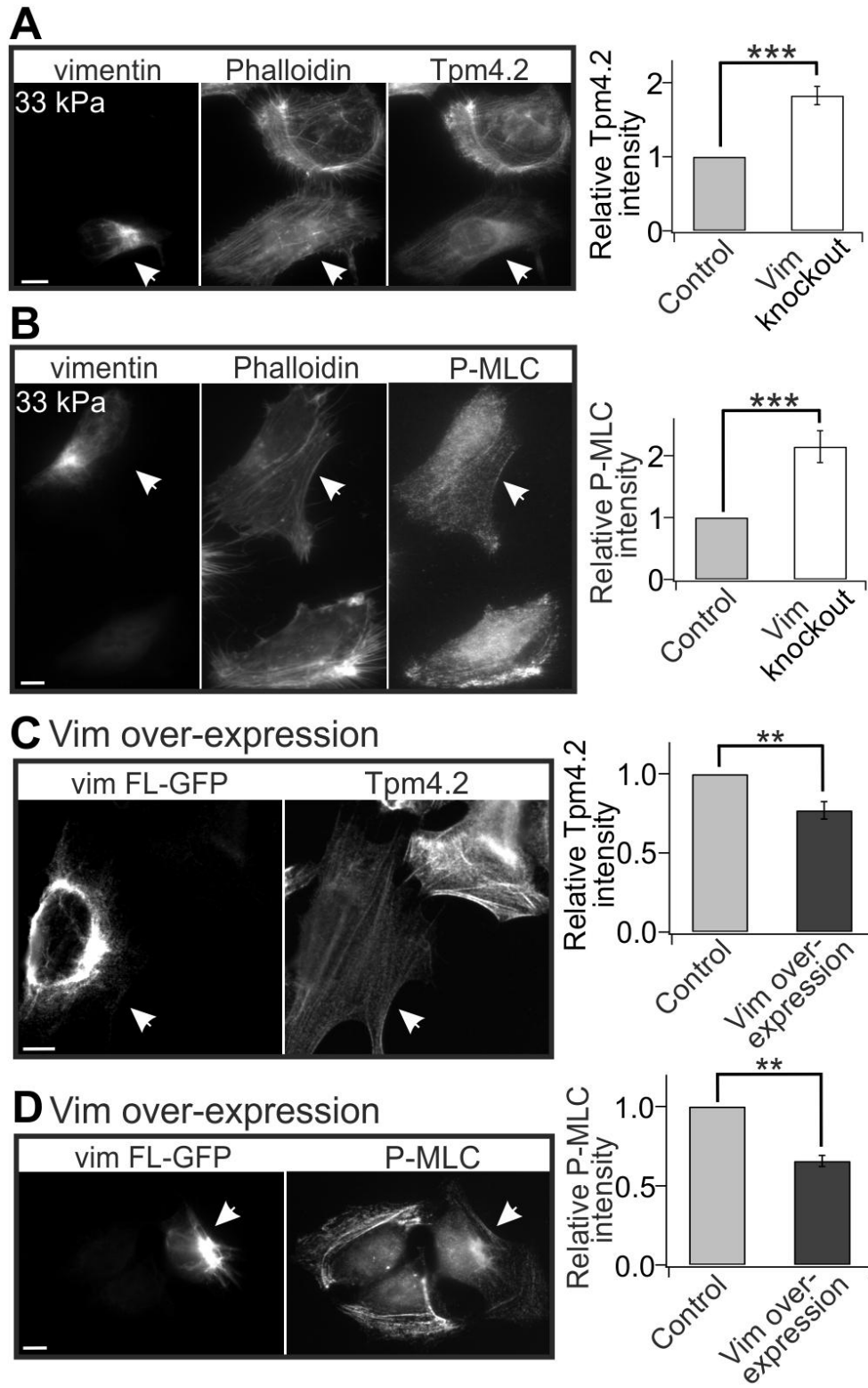


Figure S1



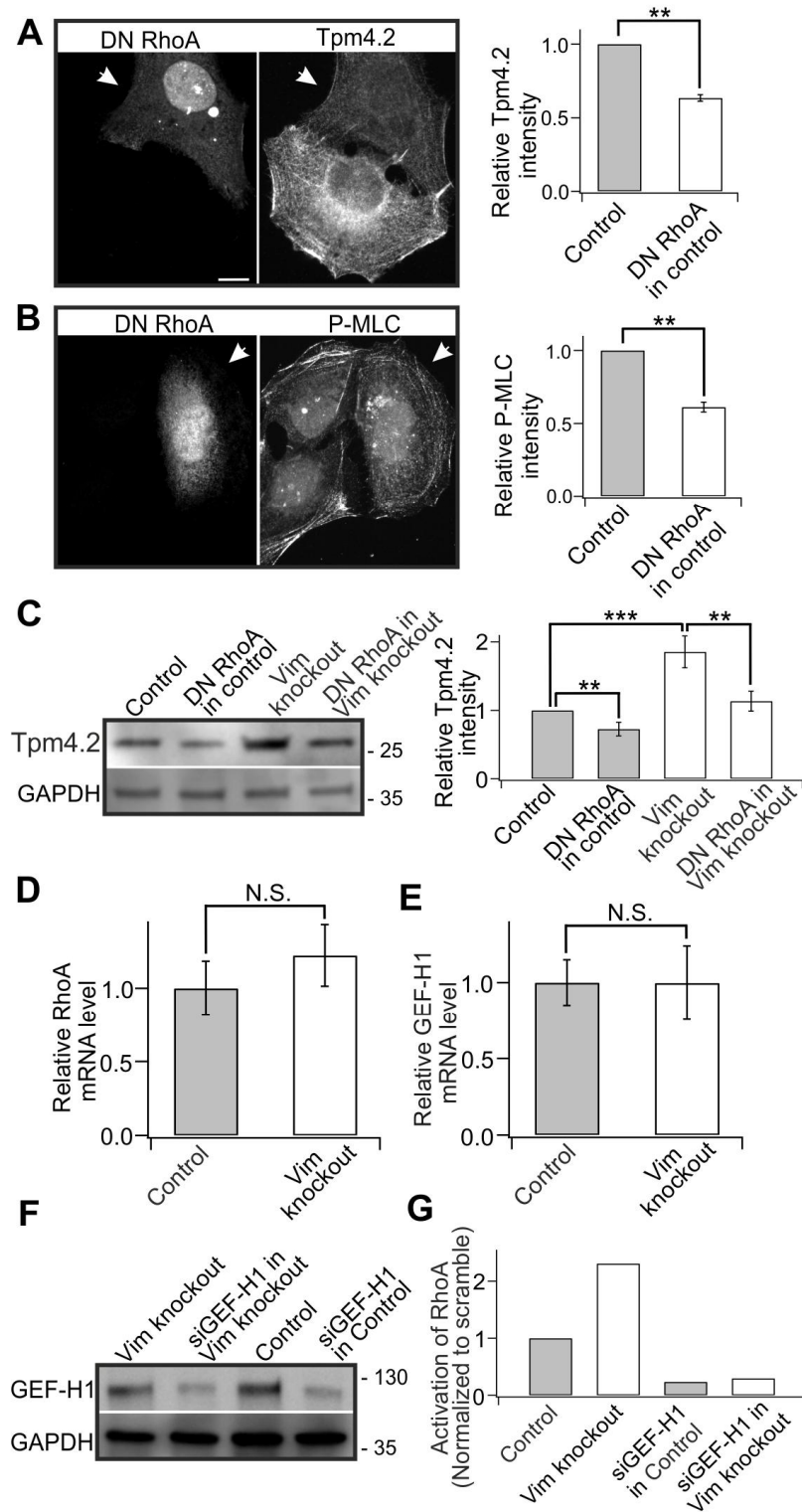
**Figure S1. Vimentin depletion results in diminished turnover of Tpm4.2 protein.** (A). Quantitative RT-PCR (qRT-PCR) analyses of Tpm4.2 mRNA levels in control and vimentin knockout cells. The data are from three independent experiments. (B). Control and vimentin knockout cells were treated with cycloheximide (CHX) and the total Tpm4.2 levels were analyzed by Western blot at the indicated time points. The blot was also probed with vimentin antibody to confirm that the vimentin knockout U2OS cell culture is not contaminated by wild-type U2OS cells, and with GAPDH antibody to control equal sample loading. Molecular weights in kilodaltons (kDa) are indicated. Relative levels of Tpm4.2 normalized to internal control GAPDH from three Western blots are shown in the graph below the blots. (C). Western blot analysis of Tpm4.2 levels in control U2OS cells and in U2OS cells incubated for 30 minutes with 10  $\mu$ M blebbistatin. The blot was also probed with actin, and GAPDH antibody to verify equal sample loading. Molecular weights in kilodaltons (kDa) are indicated. Panel on the right shows the quantification of relative levels of Tpm4.2 normalized to internal control GAPDH from three Western blots. \*\* $P < 0.01$  (paired  $t$ -test). The data are presented as mean  $\pm$  SEM. N.S. = not significant.

Figure S2



**Figure S2. Effects of vimentin on Tpm4.2 and P-MLC levels. (A, B).** Vimentin depletion results in increased Tpm4.2 and P-MLC levels also in a more compliant matrix. Panels on the left show representative images of control (indicated by arrows) and vimentin-depleted cells that were co-cultured on same plates and stained with Tpm4.2 (A) and P-MLC (B) antibodies, respectively. Panels on the right show the quantification of normalized relative Tpm4.2 (26 control cells from 9 images and 28 vimentin knockout cells from 9 images) and P-MLC (25 control cells from 9 images and 28 vimentin knockout cells from 9 images) fluorescent intensities. Mean intensity values of control and vimentin knockout cells from each image were used for statistical analysis. \*\*\* $P < 0.001$  (paired  $t$ -test). **(C, D).** Over-expression of FL-vimentin-GFP in control U2OS cells results in a decrease in both Tpm4.2 (C) and P-MLC (D) intensities. Panels on the left show representative images of non-transfected and vimentin-GFP expressing (marked with arrows) cells. Panels on the right show the quantification of normalized relative Tpm4.2 (36 control cells from 9 images and 38 vimentin knockout cells from 9 images) and P-MLC (32 control cells from 9 images and 31 vimentin knockout cells from 9 images) fluorescent intensities. Mean intensity values of control and vimentin over-expression cells from each image were used for statistical analysis. \*\* $P < 0.01$  (paired  $t$ -test). The data are presented as mean  $\pm$  SEM. Scale bars, 10  $\mu$ m.

**Figure S3**





**Figure S3. Interplay between vimentin, GEF-H1, and RhoA.** (A, B). Expression of dominant negative (DN) RhoA causes a decrease in Tpm4.2 (A) and P-MLC (B) levels in control U2OS cells. Panels on the left show representative examples of DN RhoA expressing cells (indicated by arrows). Panels on the right show the quantification of normalized relative Tpm4.2 (A, 25 control cells from 8 images and 29 DN RhoA expressing cells from 8 images) and P-MLC (B, 31 control cells from 9 images and 27 DN RhoA expressing cells from 9 images) fluorescence intensities. Mean intensity values of control and DN RhoA over-expression cells from each image were used for statistical analysis.  $**P < 0.01$  (paired *t*-test). (C). Western blot analysis verifying that DN RhoA results in a decrease in Tpm4.2 levels in both control U2OS and vimentin knockout cells. The blot was also probed with GAPDH antibody to verify equal sample loading. Molecular weights in kilodaltons (kDa) are indicated. Panel on the right shows the quantification of relative levels of Tpm4.2 normalized to internal control GAPDH from three Western blots.  $**P < 0.01$ ,  $***P < 0.001$  (paired *t*-test). (D, E). qRT-PCR analyses of RhoA (C) and GEF-H1 (D) mRNA levels in control and vimentin knockout cells. The data are from three independent experiments. (F). Western blot analysis verifying that GEF-H1 was efficiently depleted by GEF-H1 siRNA oligonucleotide (that is a different from the one used in Fig. 4) in both control and vimentin knockout cells. The blot was also probed with GAPDH antibody to verify equal sample loading. (G). G-LISA analysis of the levels of active RhoA in GEF-H1 silenced control and vimentin knockout cells generated by GEF-H1 siRNA oligonucleotides used in (E). The data are presented as mean  $\pm$  SEM. N.S. = not significant. Scale bars, 10  $\mu$ m.

**Figure S4**

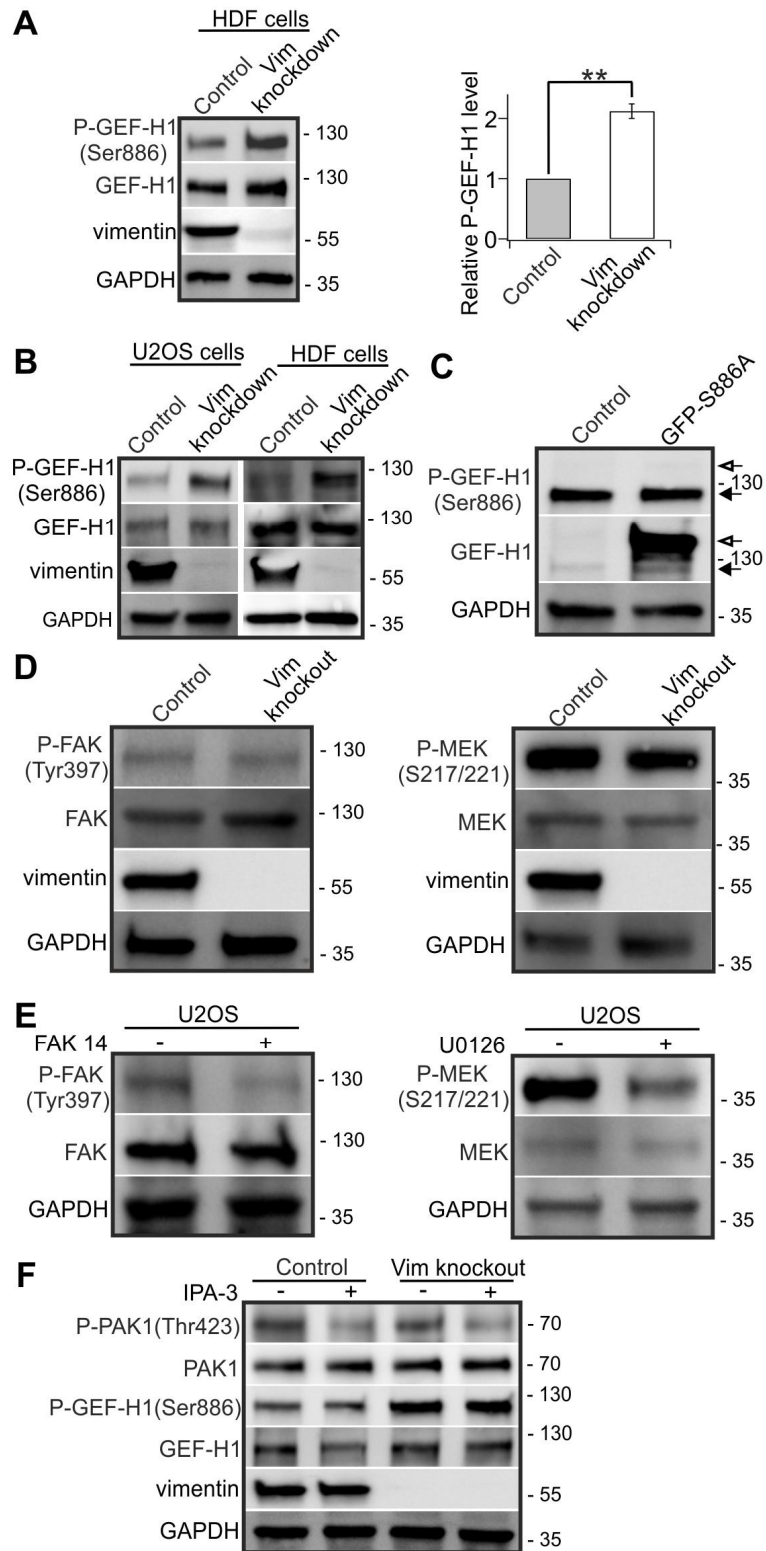


**Fig S4. GEF-H1 and kinases control experiments.** (A). Western blot analysis of GEF-H1 phosphorylated on Ser886 and total GEF-H1 levels in control and vimentin knockdown HDF cells generated using an siRNA pool as in Fig. 1B and C. Panel on the right shows the quantification of normalized relative levels of P-GEF-H1 (Ser886) compared to total GEF-H1 levels from five Western blots and presented as mean  $\pm$  SEM. \*\* $P < 0.01$  (paired *t*-test). (B). A different vimentin siRNA oligonucleotide (compared to the siRNA pool used in experiments presented in panel A) was applied to verify the vimentin knockout/knockdown induced increase in the levels of Ser886 phosphorylated GEF-H1 in both U2OS and HDF cells. (C). Western blot analysis of control cells over-expressing phospho-deficient GFP-GEF-H1 (S886A) mutant demonstrates the specificity of the P-GEF-H1 (Ser886) antibody. Black arrows show the position of endogenous GEF-H1 (~120 kDa) and hollow arrows show the position of GFP-GEF-H1 (S886A) mutant (~147 kDa). (D). Vimentin depletion drastically affected neither the total protein levels nor the levels of active FAK (left panel) and MEK (right panel). (E). Western blots verified the efficiencies of inhibitors for FAK (FAK-14, left panel) and its downstream kinases MEK1 and MEK2 (U0126, right panel), respectively. (F). Western blot analysis of P-GEF-H1 (Ser886) levels in control and vimentin knockout U2OS cells incubated in the presence or absence of PAK1 inhibitor IPA-3. The blot was probed with P-PAK1 (Thr423) and PAK1 antibodies to verify the inhibitor efficiency. The blots in (D, E, F) were probed with vimentin antibody to confirm that the vimentin knockout cell cultures were not contaminated by wild-type cells, and with GADPH antibody to verify equal sample loading. Molecular weights in kilodaltons (kDa) are indicated.